

Research Paper



Forecasting urban electric vehicle charging power demand based on travel trajectory simulation in the realistic urban street network

Eslam Mahmoudi^{*}, Tarcio Andre dos Santos Barros, Ernesto Ruppert Filho

Departamento de Sistemas e Energia (DSE), Faculdade de Engenharia Elétrica e de Computação da Universidade Estadual de Campinas - FEEC/UNICAMP

ARTICLE INFO

Keywords:
 EV Travel trajectory simulation
 Urban street network
 Urban traffic simulation
 EV user travel behavior
 Demand forecasting
 Urban charging demand

ABSTRACT

This paper presents a spatial-temporal urban charging power demand forecasting method based on EV travel trajectory simulation in the integrated urban street network and functional zones. Each EV trip is simulated via a travel trajectory based on the EV user's travel behavior, which refers to the user's decision-making processes regarding the choices of trip purpose, departure time, destination, trip route, parking time, and the time, location, and mode of EV charging. EV's daily travel trajectory is built by merging the travel trajectories of the EV's daily trips. The spatial-temporal slow and fast urban charging power demands are predicted using the simulated daily travel trajectories of available EVs in the urban area. The proposed simulation method is applied in the urban area of Campinas, Brazil. The results indicate that EVs' daily travel trajectories are realistically produced to predict the daily charging load profiles at urban activity locations and functional zones.

1. Introduction

Replacing conventional vehicles with Electric Vehicles (EVs) is unavoidable due to concerns about the depletion of fossil fuels and greenhouse gas emissions (Ternel et al., 2021). The growing EV technology, government incentives, and declining prices are anticipated to drive a steady growth in EV penetration in urban transportation systems. (De souza et al., 2018). As EVs become increasingly prevalent in urban transportation, the surge in charging demand necessitates the construction of numerous charging infrastructures within urban areas. (Fu et al., 2021). However, blindly constructing charging facilities poses significant challenges to both the transportation system and power grids (Wimbadi et al., 2021). Accurately predicting the spatial-temporal distributions of EV charging load can provide valuable insights for efficiently planning charging stations and managing urban distribution systems (Li et al., 2021). However, few studies have investigated spatial-temporal EV charging power demand prediction in urban areas. Nevertheless, the proposed approaches in these studies can no longer meet the demand for reasonable and accurate forecasts of the EV charging demands in urban areas due to the complex nature of urban electromobility. This paper aims to fill the gaps in forecasting the spatial-temporal distribution of urban charging load by comprehensively simulating the complicated EV user travel behavior in actual integrated urban street network and functional zones.

The rest of this paper is organized as follows. Section 2 reviews the related literature. Section 3 describes the research framework of the paper. Section 4 explains integrated urban modeling. Section 5 presents the travel trajectory simulation. Section 6 expresses the spatial-temporal charging load prediction model. The numerical simulation and discussion are presented in Section 7 before the concluding remarks.

2. Literature review

Large-scale penetration of EVs in the urban transportation system helps to increase energy security and reduce emissions (Bruce da Silva et al., 2022). Meanwhile, the uncertainty and flexibility of EV charging load present challenges and opportunities for the power distribution grids. On the one hand, the EV charging load brings various problems for the distribution grid, such as power quality issues (Torres et al., 2022; Rodríguez-Pajarón et al., 2021), heavy load (Mangipinto et al., 2022; Baghali et al., 2022), and power losses in the grids (Zou et al., 2020; Lebrouhi et al., 2021). On the other hand, EVs as distributed energy storage can help improve the grid's operation by providing ancillary services (Sevdari et al., 2022; Al-Obaidi et al., 2021) and increasing the integration of renewable energy sources (Salama et al., 2021; Muttaqi et al., 2019). To deal with challenges and take advantage of opportunities, a large number of studies have been conducted on optimal planning of charging stations in the power grid (Huang and Kockelman,

* Corresponding author.

E-mail address: mahmoodys546@gmail.com (E. Mahmoudi).

2020; Lin et al., 2019; Moradzadeh and Abdelaziz, 2021; Bi et al., 2021), smart charging (grid-to-vehicle(G2V)) of EVs (Fridgen et al., 2021; Spencer et al., 2021; Cui et al., 2021; et al., 2021), optimized vehicle-to-grid (V2G) (Ding et al., 2022; Li et al., 2021; Alfaverh et al., 2023), optimal coordination of V2G and G2V (Safdarian et al., 2019; Nguyen et al., 2015; Liao et al., 2021; Kasani et al., 2021), optimization of the synergies between EV and renewable energies (Zahedmanesh et al., 2021; Abbasi et al., 2019).

Extensive studies have been carried out on EV charging load modeling and simulation using two main datasets: historical charging data and travel data of conventional vehicles. The historical charging data collected from the private and public charging stations were directly employed to predict the charging load demand by using mathematical statistics (Mirzaei et al., 2016), data-driven methods (Zhiyan et al., 2022), neural networks (Chang et al., 2021), and machine learning methods (Yi et al., 2022; Zhang et al., 2021; Zhao et al., 2021).

The travel datasets used in the literature mainly include household travel survey data (e.g., National Household Travel Survey (NHTS) (NHTS, 2017)), Origin-Destination (OD) travel data (Chen et al., 2020), and vehicle GPS data (Brady and O'Mahony, 2016). The travel data was used to develop the probabilistic models of EV travel parameters such as trip start and end times, travel distance, driving time, etc. With these probabilistic inputs, the approaches like Monte Carlo simulation (Yue et al., 2019; Yan et al., 2020; Zhang et al., 2020; Su et al., 2019), Markov chain (Gruosso and Gaiani, 2019; Han et al., 2020), Markov chain Monte Carlo (Wang and Infield, 2018; Iwafune et al., 2020), trip chain (Wang et al., 2017; Yang et al., 2016; Chen et al., 2015; Haiyang et al., 2019), Markov decision process (Tang and Wang, 2016; Zhang et al., 2018) kernel density estimation (Paterakis and Gibescu, 2016), OD matrix (Xia et al., 2019), state-space model (Iversen et al., 2017) have been employed to predict EV charging demands. Furthermore, the queueing theory was also used in some studies (Esmailirad et al., 2021; Xiao et al., 2020; Kumar et al., 2022) for predicting the EV charging demands at charging stations by anticipating the EV arrival rate at the stations with the Poisson distribution.

The increasing presence of EVs in urban areas highlights the need for models that can accurately predict both slow and fast charging demands, considering the uniqueness of urban spatial characteristics. However, there is a notable gap in the simultaneous prediction of spatial-temporal distributions of slow and fast EV charging power demands within the integrated spatial framework of urban street networks and functional zones.

In recent years, several studies have proposed models aiming to forecast EV charging demand in urban areas. While the majority of research in this domain has concentrated on optimal charging station planning (Cui et al., 2019; Kavianipour et al., 2021; Fazeli et al., 2021; Zhu et al., 2023), there is also been a separate focus on forecasting and analyzing the spatiotemporal characteristics of EV charging loads in urban areas. Mu et al. (2014) developed a spatiotemporal model to evaluate the impact of large-scale EV deployment on the distribution network of an assumed urban area divided into residential, commercial, and industrial zones. In (Arias et al., 2017), the fast charging demands at the Fast Charging Stations (FCSSs) located at some road network nodes inside the metropolitan area of Seoul were predicted based on the real-time closed-circuit television data from an urban traffic network. Li et al. (2018) proposed a spatial-temporal charging load forecasting model in which two trip chains simulate daily EV trips with two and three trips between home, work, and else in an assumptive street network graph, including 72 road nodes and 122 paths. In (Shepero and Munkhammar, 2018), the GIS data of the urban area was used to cluster urban functional zones and proposed a spatial Markov chain model to estimate the charging demand profiles at different parking lots. Xing et al. (2019) proposed a data-driven approach to predict the spatial-temporal EV charging demand in residential, commercial, industrial, and public zones by mining ride-hailing trip data and modeling the single EV. Yi et al. (2019) assumed a hypothetical urban area

containing several zones to predict the spatial-temporal EV charging load at the zones, in which the traffic densities of roads are taken as constant values to determine the EV speed based on a simple speed-flow model. In (Ge et al., 2020), a spatiotemporal distribution prediction method for EV charging loads was developed based on the improved random forest to forecast the spatial and temporal distribution of EV cluster load in an urban area. Xing et al. (2020) introduced a data-driven approach incorporating human decision-making behavior to develop a model to forecast the fast-charging demand in the urban network of Nanjing, China. Wang et al. (2023) proposed the use of a heterogeneous spatiotemporal graph convolutional network to predict electric vehicle charging demand in Beijing, considering various grid scales. Shafaqat and Liu (2023) analyzed the spatial-temporal forecasting strategy for EV charging demand, assessing performance from both power systems and urban transportation system perspectives in a hypothetical scenario.

Straub et al. (2023) introduced an activity-based model designed to estimate the spatial and temporal distribution of EV charging demand throughout the day in the urban area of Berlin. Their study encompassed three charging scenarios: home-charging, work-charging, and shopping-charging. Zhang et al. (2023) presented a trip-chain-simulation-based charging demand prediction model, enabling a quantitative exploration of the spatiotemporal distribution of charging demands in Beijing. The model employed a spatial resolution of 0.46 km hexagonal units and a time resolution of 15 minutes. Liangliang et al. (2023) employed a graph convolutional network (GCN) in conjunction with the Transformer to extract spatiotemporal features in their study of spatial-temporal EV charging demand forecasting in an urban area of Palo Alto, USA.

The literature review shows that while the current research on the prediction of EV charging loads has addressed various factors influencing the spatiotemporal EV charging demands, there are challenges in applying these methods to predict the spatial-temporal urban charging load. The main issues of previous studies are as follows.

- The historical data-based forecasting models used in studies (Yi et al., 2022; Zhang et al., 2021; Zhao et al., 2021) can only be used for specific charging locations from which the data comes, making the models less scalable.
- The two main frameworks for EV mobility simulation in studies, including virtual network (Yan et al., 2020; Zhang et al., 2020; Han et al., 2020; Iwafune et al., 2020; Haiyang et al., 2019) and small graph (Arias et al., 2017; Li et al., 2018; Mu et al., 2014; Yi et al., 2019; Yue et al., 2019) represent oversimplification models of the urban area, which consists of many street segments and diverse land uses.
- The travel distance and travel time modeling solely based on the travel data in studies (Yan et al., 2020; Haiyang et al., 2019; Paterakis et al., 2019; Zhang et al., 2020; Yan et al., 2020; Iwafune et al., 2020) are inadequate for accurately simulating urban EV mobility. Because these travel parameters are highly affected by the spatial structure of the urban area, dynamic traffic of the streets, EV driving speed, etc.
- Although street traffic strongly affects driving speed, driving time, EV energy consumption, and thus EV charging demand, it has been ignored in most studies (Yan et al., 2020; Yi et al., 2019; Zhang et al., 2020). However, in some studies (Arias et al., 2017; Xia et al., 2019; Yi et al., 2019), the street saturations in a period were set to a constant value, assuming that the saturation of different roads has a generally consistent temporal trend.
- The EV user travel behavior was ignored in many studies (Zhang et al., 2020; Haiyang et al., 2019; Yan et al., 2020), and they only rely on travel data to model the EV travel parameters. However, in some studies (Li et al., 2018; Yi et al., 2019; Yue et al., 2019), simple models were considered to simulate user travel behavior. In these studies, trip destinations were randomly selected from the graph's nodes, and trip routes were determined as the shortest or fastest

paths to the selected node. Whereas EV users' travel behavior in the trip's destination and route choices is significantly affected by their preferences, the spatial characteristics of the urban area, dynamic traffic of streets, and EV energy consumption.

- In most studies (Xia et al., 2019; Zhang et al., 2020; Han et al., 2020; Yan et al., 2020), the EV trip's energy consumption was estimated as constant per kilometer (kWh/km). While EV energy consumption mainly depends on EV technical specifications, driving speed, street slopes, etc. Thus, underestimating or overestimating EV energy consumption leads to inaccurate EV charging demand prediction.
- The trip chains used in studies (Shepero and Munkhammar, 2018; Xia et al., 2019; Wang et al., 2017; Chen et al., 2015) to model the EV daily trips were simple trip chains consisting mainly of three destinations home, work, and Others. Furthermore, EV charging demands were only predicted at private charging locations (e.g., homes or workplaces) or public charging stations, considering fixed charging start times. While, in the daily travel of EVs in the urban area, there is the possibility of EV charging at any time and location, such as homes, workplaces, shopping malls, recreations, FCSs, etc.

In summary, the relatively high complexity of the actual urban street network and its dynamic traffic, the high diversity of urban land uses, and the complicated travel behavior of the EV user are expected to pose serious challenges for employing the models and approaches of existing studies in charging demand prediction of EVs in the urban areas. Compared with existing studies, the main contributions of this paper are summarized below.

- (1) Unlike the oversimplified models of urban areas (i.e., virtual network and small assumptive graph) in previous studies, this paper creates the actual urban spatial model based on the real-world data of the urban streets and functional zones. The urban integrated model is developed by combining the urban street network graph and urban functional zone polygons.
- (2) To overcome the issue of ignoring or assuming constant values for street congestion levels in previous studies, this paper develops a new web-based tool to collect real-world traffic data of urban street segments from Google Map Traffic Layer (GMTL). This tool automatically captures the GMTL's map images and specifies the traffic congestion of the street segments according to the corresponding traffic colors determined by processing the captured images.
- (3) Contrary to the existing studies, the EV user travel behavior is comprehensively simulated by models that predict the purpose, departure time, parking time, destination, optimal route, and energy consumption of each EV trip, as well as the time, location, mode, and amount of the possible charging demand at the trip destination. The first departure time from home, trip purpose, and parking time are probabilistically modeled based on travel data of the urban area. The trip destination choice model is developed based on the Gravity model according to the geospatial characteristics of the urban area and the attractiveness of urban functional zones specified from travel data. The dynamic trip route choice model, including pre-route planning and en-route replanning, is developed to choose the minimum-energy trip route on the urban street network. In contrast to the assumed constant kWh/km of EV energy consumption in previous studies, the EV energy consumption is estimated by a segment-based EV energy consumption model formulated based on actual EV specifications, average EV driving speed, and average slopes of street segments, in which the average EV driving speed is specified according to the traffic conditions and the speed limits of the streets and the average slopes of street segments are estimated based on open-source Digital Elevation Model (DEM) data. Furthermore, the EV user charging decision at the destination is modeled based on range anxiety and a Fuzzy decision system.

- (4) This paper presents a novel simulation framework for forecasting the spatial-temporal distribution of urban charging power demands by simulating EV trips with realistic travel trajectories in the integrated framework of urban streets and functional zones. Each EV trip is simulated based on the EV user's travel behavior via a travel trajectory that specifies the spatial-temporal attributes of driving, charging, or parking, as well as energy consumption, SoC profile, and charging demand of the trip. Accordingly, by combining the travel trajectories of EVs' daily trips, their daily travel trajectories are simulated in a multi-location and multi-purpose framework to predict the spatial-temporal distributions of the urban area's slow and fast charging demands in different locations and functional zones.

3. Research framework

The city's planners and decision-makers can leverage predictions of spatial-temporal distribution of urban charging demands to deploy urban charging infrastructures, thus promoting urban electromobility effectively. However, obtaining real-world data on the city-scale spatial-temporal distribution of charging demands for a high EV penetration level is often challenging. In such cases, simulation-based methods can serve as valuable tools for forecasting the spatial-temporal distributions of urban charging loads.

This paper aims to forecast the spatial-temporal distribution of urban charging load across urban activity locations and functional zones. To achieve this, the daily travels of EV users are simulated within a multi-purpose, multi-location framework to identify the timing, location, mode, and amount of EVs' charging demands. To enhance the realism of the proposed simulations, various real-world datasets are employed, which encompass OpenStreetMap (OSM) data (OpenStreetMap, 2024), traffic data from Google Maps, urban land use data, Digital Elevation Model (DM) data, travel data, demographic and census data, and EV specification data.

Geospatial data from OSM is utilized to create the urban street network, where each street segment is represented as a line connecting two intersection nodes defined by latitude and longitude (Lat/Long). The functional zones are specified by polygons whose vertices are determined by specific Lat/Longs extracted from land use data.

The integrated urban model is developed by incorporating the street network and functional zone polygons to provide a spatial framework for simulating EV trips. The street network establishes the connectivity between Origin-Destination (OD) locations, specified by certain Lat/Longs within the functional zone polygons and next to the OSM street segments. Within this integrated framework, the travel data is employed to simulate the EV user travel behavior using various models that determine the departure time, trip purpose, destination location, route, and parking time of the trip, as well as the time, location, mode and amount of possible EV charging events. The departure time from each activity location, except the first departure time from home, is calculated by summing the arrival time at the destination with the corresponding parking duration. The first departure time from home, which is not influenced by urban spatial structure and traffic patterns, is modeled probabilistically using travel data. The EV trip purpose is specified using a stochastic trip purpose prediction model developed based on travel data. EV trip's destination is predicted by a doubly constrained gravity model developed based on travel data and trip production and attraction of urban zones. The optimal route for the EV trip on the OSM street graph is forecasted by a dynamic minimum-energy route planning model developed in accordance with dynamic urban traffic and EV energy consumption. The dynamic traffic pattern is simulated using traffic data collected from GMTL. The energy consumption of EV driving on the streets is estimated by an EV energy consumption model developed based on the actual EV specifications, driving speed, and the street slopes calculated based on DEM data. The EV driving speed on urban streets is estimated according to the speed

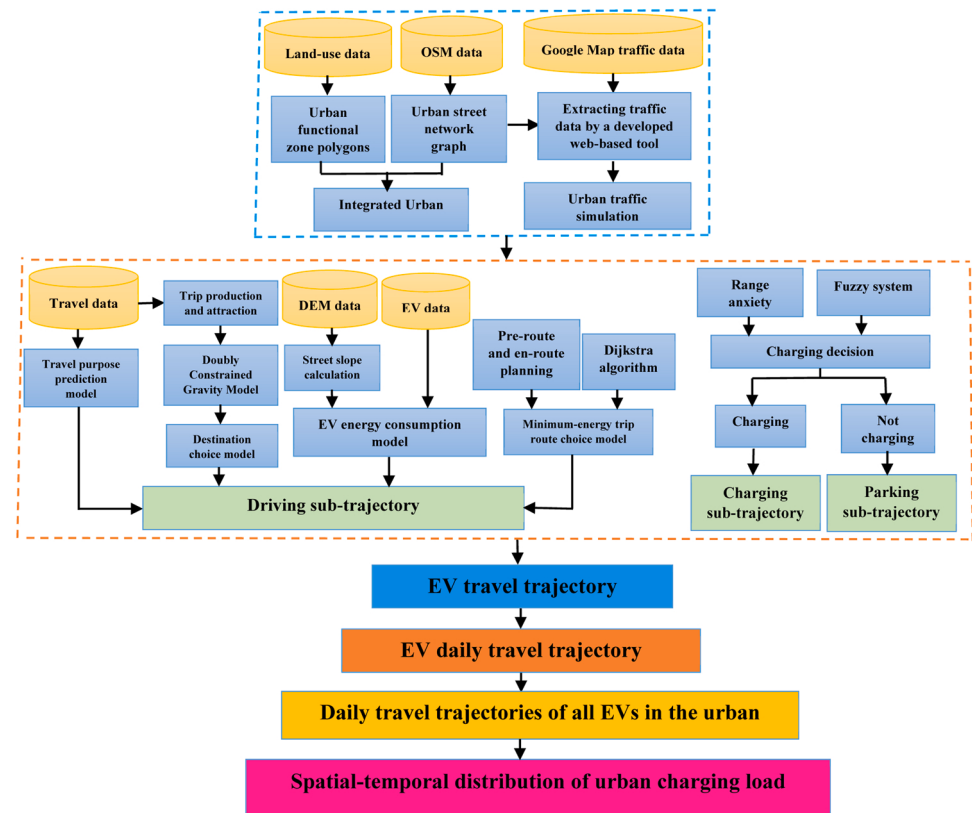


Fig. 1. The flowchart of the research framework.

limit and street traffic. The driving time is calculated based on the EV driving speed and lengths of street segments. The EV arrival time at the destination is calculated as the sum of travel time and the origin's departure time. The parking time at activity locations, independent of urban spatial structure and traffic pattern, is modeled probabilistically using travel data. The time, location, and mode of EV charging are simulated using decision models developed based on factors such as range anxiety, the required energy for their next trip, parking time, etc.

Each EV trip, including driving and subsequent charging or parking, is modeled based on EV user travel behavior within the integrated urban framework. The trip begins at the departure time from the origin, follows the minimum-energy trip route to the chosen destination, and ends at the destination. Upon arrival at the destination, the user decides whether to charge the EV. In the case of charging, the EV will be charged during the parking period at the destination. Otherwise, it will be idle.

Therefore, an EV trip consists of a sequence of spatial nodes with their time stamp, including OD locations and street intersections of the trip route along with departure time from the origin, times to reach or leave the street intersections, and arrival time at the destination. Therefore, the spatiotemporal characteristics of an EV trip can be described by a travel trajectory, representing three typical EV behaviors: driving, parking, and charging. These three behaviors can be thought of as three states that an EV traverses over time. Moreover, travel trajectory includes the profiles of speed, energy consumption, and SoC of EV driving, as well as time, location, mode, and amount of EV charging in the trip.

The daily travel trajectory of each EV user is built by merging the trajectories of EV trips with different purposes. The spatial-temporal distribution of EV charging load at the urban locations and functional zones is predicted based on simulated daily travel trajectories of all EVs in the urban area. Fig. 1 shows the flowchart of the proposed research framework.

4. Integrated urban model

The integrated urban model is created by merging the street network graph and urban functional zone polygons, utilizing the data from OSM and the land use datasets.

4.1. Urban street network

To provide a spatial framework for EV mobility modeling in the EV travel trajectory simulation, an urban street network is modeled based on the geospatial data of the OSM (OpenStreetMap contributors, 2022).

4.1.1. Urban street graph

As the OSM data cannot be automatically extracted into a graph, an interface with computing environments (like MATLAB) is required to process the OSM data and create the street network graph. The procedure for constructing the street network graph based on OSM data is described below.

- (1) The OSM data of the study area is imported in MATLAB, and a parsing script extracts the information contained in the files.
- (2) The OSM ways that contain a 'highway' tag are extracted as street segments.
- (3) The street segments are classified into the trunk, motorway, primary, secondary, tertiary, residential, etc.
- (4) The street segments are corrected for possible geometry and topology problems.
- (5) A square adjacency matrix is generated, in which the corresponding entry of two intersection nodes of street segments is one if they are connected and zero otherwise.
- (6) The fully connected street network graph is created based on the adjacency matrix and the Lat/Longs of street intersection nodes.

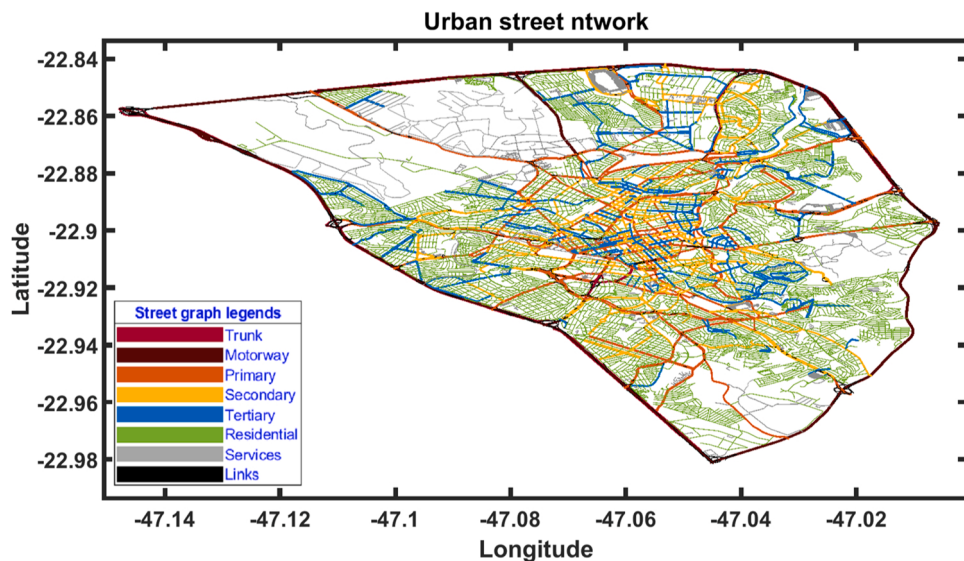


Fig. 2. Urban street network graph of the study area.

Fig. 2 shows the street network graph of the study area, which is the urban area of Campinas, Brazil. The area of the study area is 116.525 km^2 . The urban street network graph includes 113,062 street segments (edges) and 49,532 intersections (nodes).

4.1.2. Traffic simulation of the urban street network

In this paper, the constructed OSM urban street network makes it possible to collect traffic data from mapping systems such as Google Maps. Customizable, scalable, and cost-effective traffic data can be obtained using Google Maps. The GMLT does not provide the street traffic dataset. Instead, it represents the streets' traffic conditions in colors of white, green, orange, red, and dark red, defining no traffic, smooth traffic, moderate traffic, heavy traffic, and traffic jam, respectively. Hence, a novel web-based tool is developed to collect the daily traffic data of OSM streets by processing the captured GMLT images over the day. This tool consists of three steps which are explained below.

(1) Identifying street pixels corresponding to OSM street segments

The OSM street network and GMLT map images are matched to determine the street pixels corresponding to each OSM street segment. For this purpose, firstly, the GMLT images that only contain streets without additional information (e.g., the street name, location name, bus stops, etc.) are captured with a zoom level of 15. Since only one image of a zoomed-in map cannot cover all streets of the study area, the six images of the GMLT map should be captured to cover the study area. Secondly, the street pixels of captured images are extracted, and by manually cleaning and incorporating the pixels, a street network equivalent to the OSM street network is created. Finally, the street pixels are matched by the OSM street network to identify the street pixels corresponding to each street segment. These are the pixels surrounded by the created rectangular buffer around the segment. **Fig. 3** shows the process of identifying street pixels corresponding to each OSM street segment.

(2) Automatic capturing of the traffic images at each time-step

The GMLT updates the traffic color of the streets every moment. Assuming that a street segment's traffic condition can stay unchanged over a short time, a time-step is considered to capture the GMLT images and collect daily traffic data. The six JavaScript files are created to load the web pages of six GMLT images that cover all streets of the study area specified by traffic

colors without any additional information on the images.

At the beginning of each time-step, the tool automatically captures screenshots of the GMLT images using the Java robot and web reader of MATLAB. For this, the web reader reads the JavaScript file of each map image, and the 2-second pause is imposed to ensure that the map is loaded with the updated traffic information. Then the Java-robot captures a screenshot of the web map image and is saved in the image data format corresponding to the step-time. This process is repeated for each map image of the study area and each time-step of the day.

(3) Processing of captured images to specify traffic colors of OSM street segments

For each time-step, the pixel coordinates of streets are extracted by processing the corresponding saved image data files. Then, the extracted colored pixels are incorporated to create a colored street network equivalent to the OSM street network. Finally, the equivalent colored street network and street segments' rectangular buffers are matched to specify the traffic color of each street segment, which is the dominant color of colored pixels surrounded by the street segment's buffer. **Fig. 4** shows the process of identifying traffic colors of street segments.

Therefore, at each time-step the traffic color of each street segment is determined and stored with a numeric value of 1, 2, 3, 4, and 5 for smooth traffic, moderate traffic, heavy traffic, traffic jam, and no traffic, respectively.

By considering the time-step of two minutes for traffic simulation, the traffic data for a weekday are collected by the developed tool from 5:00–5:00 of the next day, resulting in obtaining the traffic data for each street segment comprising 720 numbers of 1–5.

4.2. Urban zoning

In this paper, the urban area is divided into functional zones to specify the activity locations, which are the potential destinations of EV trips. Moreover, the urban area is also divided into Transportation Analysis Zones (TAZs) to enable the use of the study area's travel data, which is spatially collected at the TAZ level, in EV travel trajectory simulation.

4.2.1. Urban functional zones

According to the land use data of Campinas ([SEPLAMA, 2022](#)), the study area is classified into five functional zone groups: residential, commercial and service, industrial, social and service, and mixed zones.

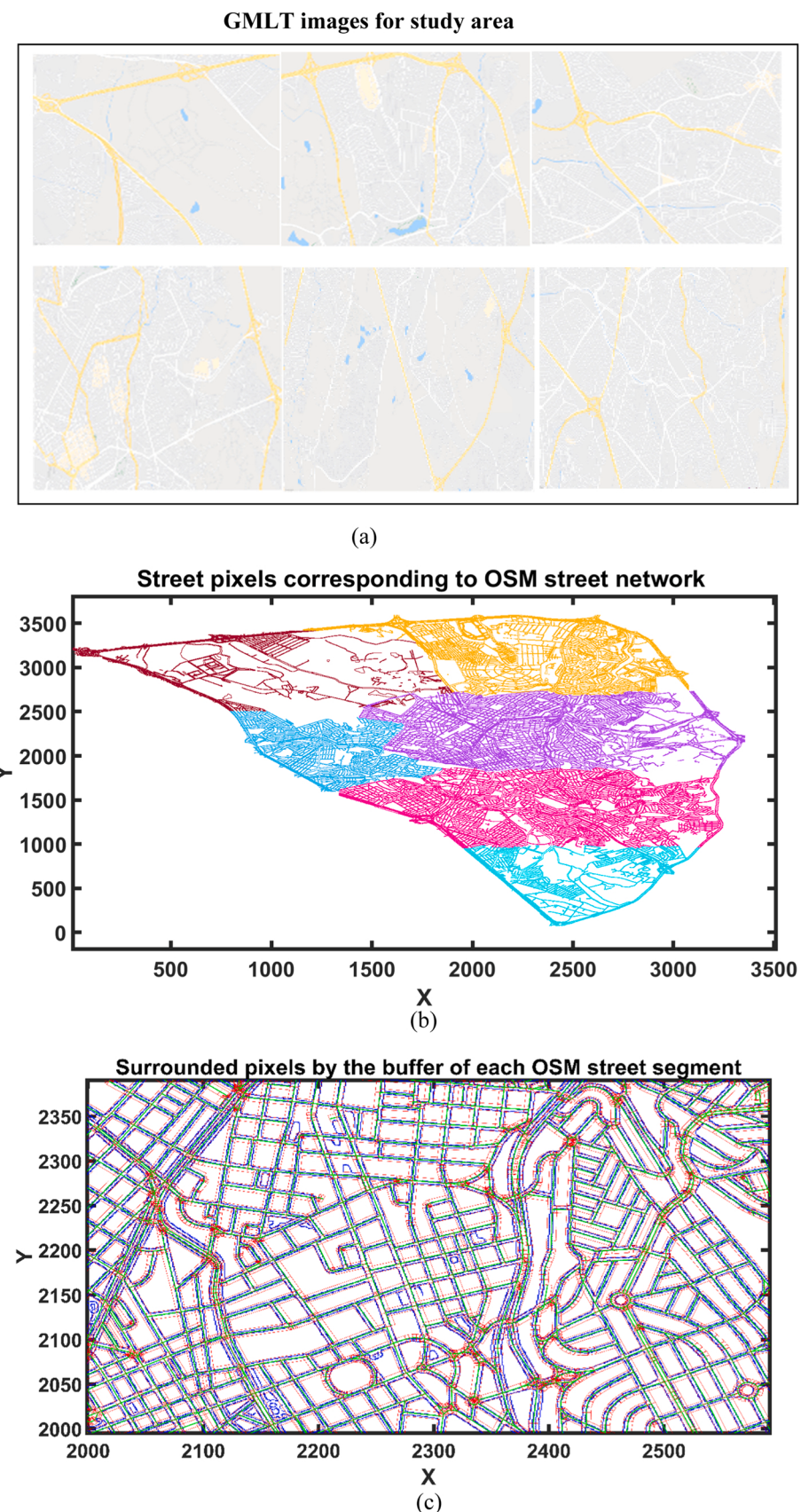


Fig. 3. Process of identifying street pixels corresponding to each OSM street segment. (a) GMLT images of all urban streets, (b) OSM street pixels, and (c) rectangle buffers corresponding to OSM street segments.

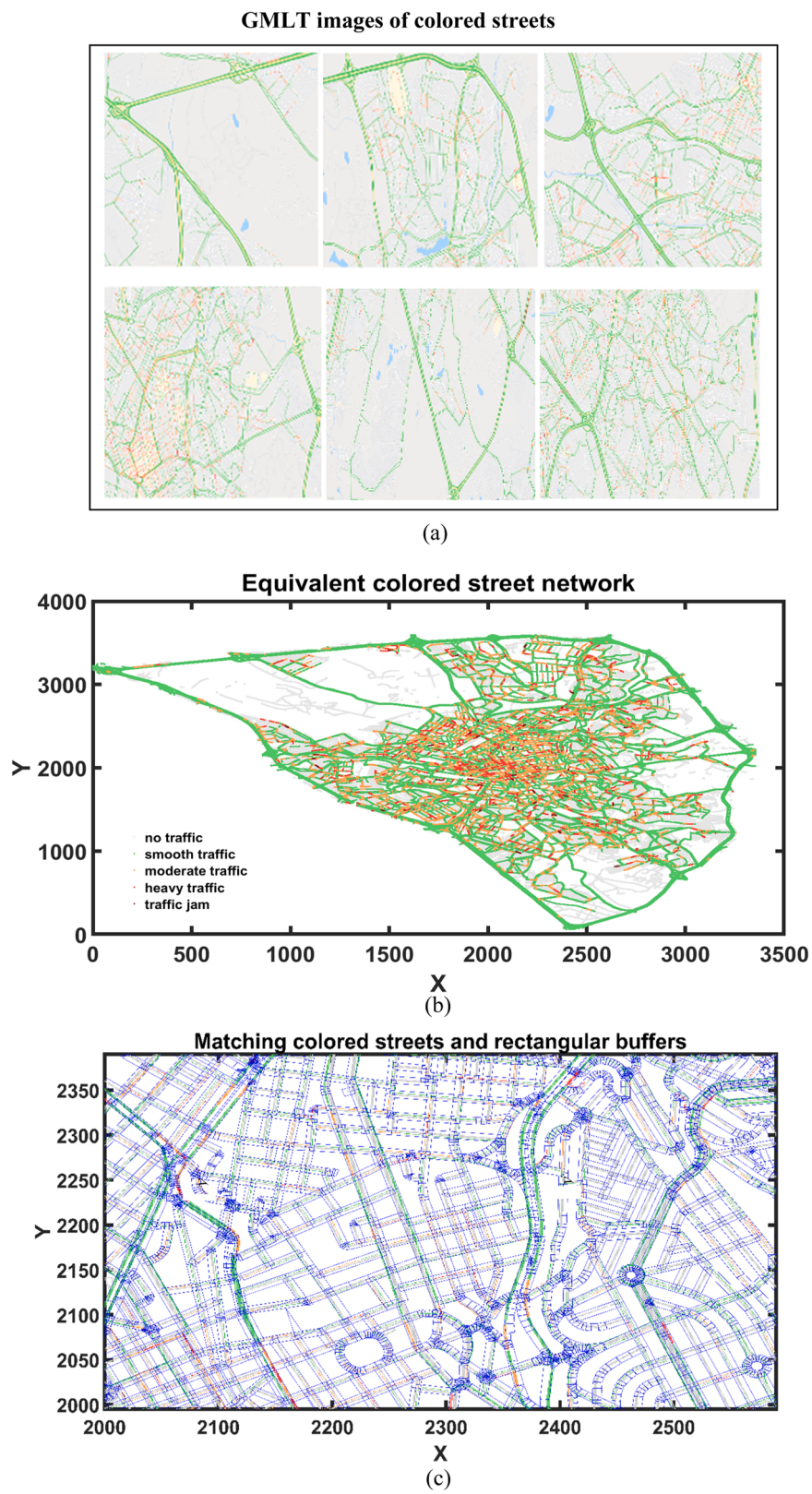


Fig. 4. Process of specifying traffic colors of street segments:(a) GMLT images of colored streets, (b) colored street pixels, (c) rectangle buffers matched with colored pixels.

The residential zones include three subgroups: residential zones with predominant single families (residential-G1), multiple families (residential-G2), and single and multiple families(residential-G3). The commercial and service comprise the city center area, business and

service, shopping mall, and supermarket. Social services group consists of education, health, leisure, culture, sport, institutions, parks, and green areas. The mixed zones include residential-commercial (RC), residential-industrial (CI), commercial-industrial (CI), and

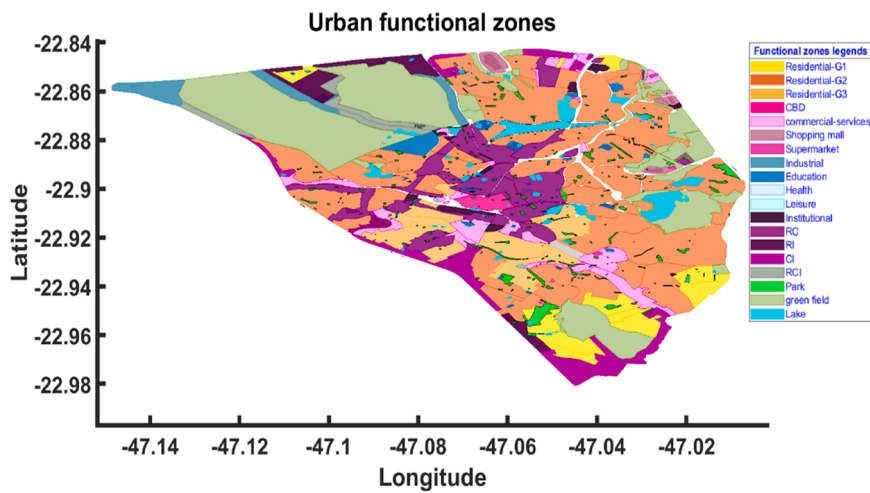


Fig. 5. Urban functional zones of the study area.

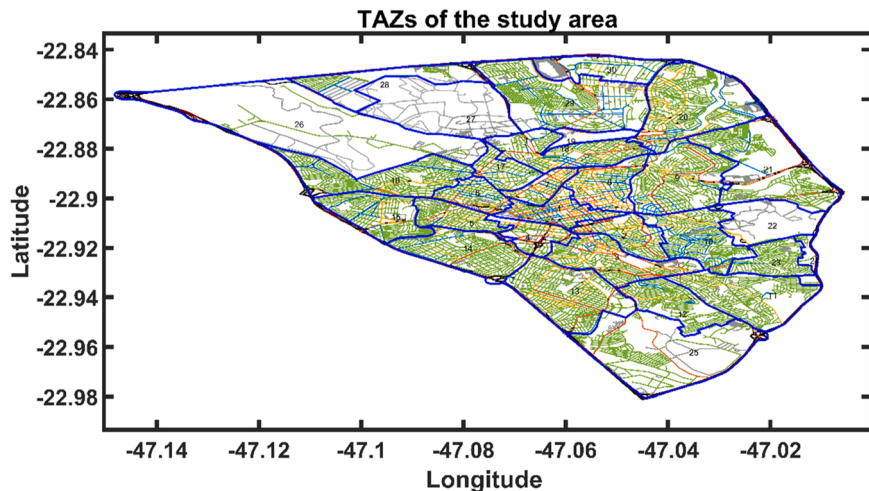


Fig. 6. TAZs of the study area.

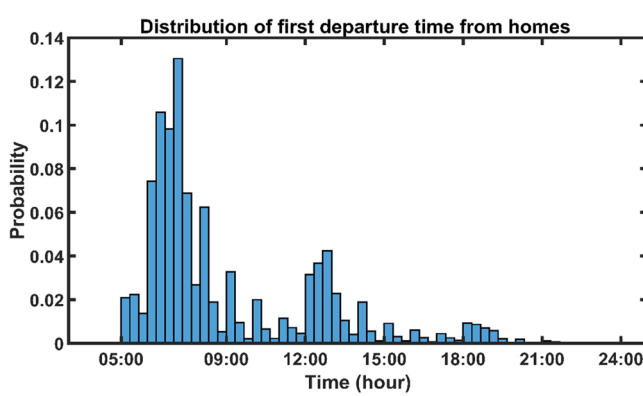


Fig. 7. Distribution of the first departure time from home data in the study area.

residential-commercial-industrial (RCI). Fig. 5 shows the functional zones of the study area, in which polygons outline the functional zones. The polygons, whose vertices are specified with Lat/Longs, determine the boundaries of functional zones in the urban area.

4.2.2. Transportation Analysis Zone

The travel data of the study area is extracted from the Origin and Destination survey of the Metropolitan Region of Campinas (OD-MRC), which is provided by the Metropolitan Transportation Secretariat of São Paulo (MTSSP) (STM, 2022). The travel data comprises the spatial and temporal information of the city population's daily travels. The trips' spatial characteristics are the TAZs of the trips' OD, and the temporal attributes include the trips' start and end times and dwelling times at the destinations.

The study area consists of 30 TAZs that are represented by polygons. Fig. 6 shows the TAZ polygons of the study area.

5. Travel trajectory simulation

For each EV trip, the departure time, trip purpose, and destination location are determined before starting the trip, and then the trip is simulated with a travel trajectory in the sub-trajectories of driving, charging, or parking. In the following subsections, the stochastic trip purpose prediction model, probabilistic departure time model, destination choice model, and the simulation of the travel sub-trajectories are explained in detail.

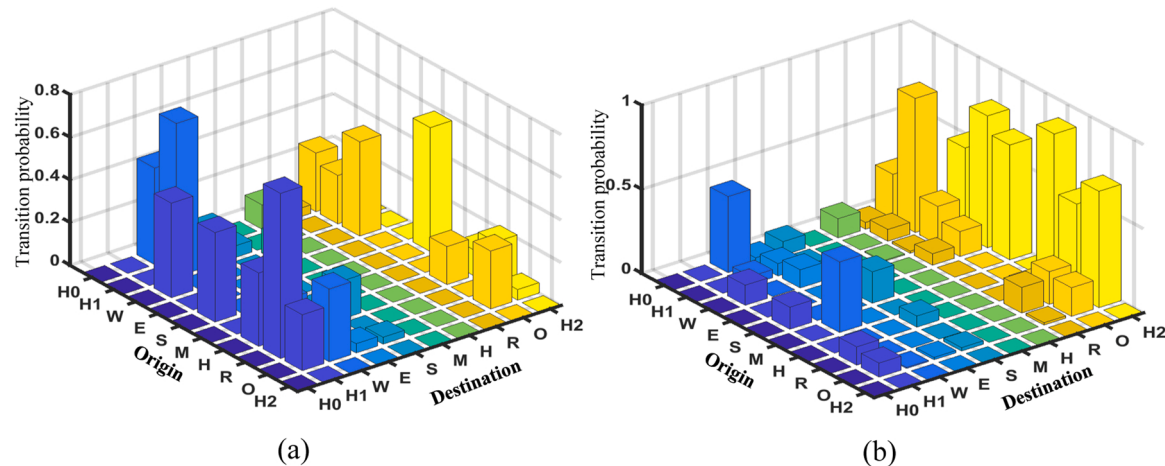


Fig. 8. Spatial transition probability matrixes; (a) 8–9 o'clock, (b) 17–18 o'clock.

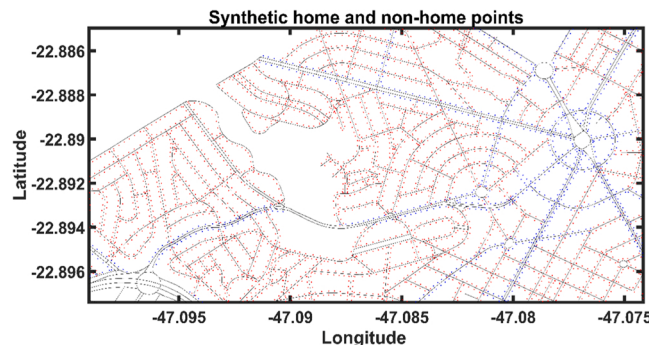


Fig. 9. Synthetic home and non-home points in a sample area.

5.1. Probabilistic model of the first departure time from home

In this study, EV daily trips are considered home-to-home trips in which the EV departs from home at a specific time, makes several trips between different activity locations in the urban area, and finally returns home. Hence, except for the departure time of the first trip that starts from home, the departure time from an activity location is the sum of the arrival and parking times at the location. The first departure time from home, independent of stochastic urban transportation, is modeled probabilistically by a Probability Distribution Function (PDF) to represent the stochastic nature of EV daily trips. To this end, the first departure time from home data is extracted from the OD-MRC dataset to calibrate a PDF. Fig. 7 shows the distribution of the study area's first departure time from home data. The first departure time from home is modeled by a Generalized Extreme Value (GEV) PDF with $k=0.2515$, $\sigma=111.2026$, and $\mu=436.4786$ (in minutes).

5.2. Stochastic trip purpose prediction model

The purpose of each EV trip represents the activity that will be performed at the destination location. Since EVs are not yet widespread in the study area, assuming that EVs have the same travel patterns as conventional vehicles, the cars' travel data of the study area is used to develop the EV's trip purpose prediction model based on the Markov chain concept. To this end, the hourly Transition Probability Matrices (TPMs) are calculated based on transferring frequencies between different purposes collected from the OD-MRC at one-hour intervals. The trip purposes defined in OD-MRC are home (H), Work (W), Education (E), Shopping (S), Meals(lunch) (M), Health (H), Recreation (R), and Others (O). In the daily itinerary, home is divided into three purposes:

starting the trip from home (H_0), short stay at home during the daily trips (H_1) and end of daily trips at home (H_2). Therefore, by considering the 24-hour day and the ten trip purposes ($H_0, H_1, H_2, W, E, S, M, H, R$, and O), 24 hourly TPMs with square size 10×10 are generated. For instance, Fig. 8 shows the TPMs for 8:00–9:00 and 17:00–18:00.

Therefore, at the departure time of each trip's origin, the trip purpose is stochastically determined based on the probabilities corresponding to the origin's activity type extracted from the hourly TPM respective to the departure time. Note that the number of daily EV trips is not predefined for EVs. Instead, daily trips start from home, the trip purpose is predicted at the departure of each location, and the daily itinerary is finished when the trip purpose will "ends at home" purpose. Moreover, it is not specified in advance whether EV users are employed or unemployed, and employees are those who make a trip for work purposes.

5.3. Destination choice model

The daily travels of EV users are made to perform a set of activities at different locations in the urban functional zones. The activities are classified into two types: activities at fixed locations and activities at non-fixed locations. From the defined trip purposes, Home, Work, and Education are activities with fixed locations, and Shopping, Meals, Health, Recreation, and Others are those with non-fixed locations. The activity locations can be specified by Lat/Long coordinates in the modeled urban functional zone polygons. However, due to the lack of Lat/Longs data on the activity locations in the study area, they are synthesized in the corresponding functional zones.

5.3.1. Synthesize activity locations in urban functional zones

Home and non-home points (e.g., workplaces, shops, etc.) are generated next to residential and non-residential streets (i.e., tertiary, secondary, and primary streets) to synthesize activity locations in the functional zones. To this end, hypothetical lines are considered in parallel to the OSM streets, and the points are generated on these lines, in which the distance between two consecutive points is extracted from the uniform distribution $U(20–50)$ and $U(50–250)$ for home and non-home points, respectively. For instance, Fig. 9 shows the synthetic home and non-home points in a residential zone.

5.3.2. Assigning the fixed activity locations to the EV users

In the travel trajectory simulation, no destination choice is made for a trip with the purpose corresponding to a fixed activity location. Instead, the trip's destination is a fixed location previously assigned to the EV user. The assignment of fixed locations for Home, Work, and Education to EV users is described in the following.

(1) Home locations

A home is assigned to each EV user from the synthesized home points. Due to the price of the EV, it is assumed that the higher income households are more likely to have an EV. Hence, based on households' income data extracted from the Campinas's census data (IBGE, 2022), the study area is divided into three groups of high, medium, and low income areas, and EVs are randomly assigned to home points in these areas with percentages of 60%, 30%, and 10%, respectively.

(2) Workplace locations

To each EV user who makes a trip with a Work purpose, a workplace is assigned according to the data of work types and work trips in the study area. Eight work types specify the users' work types: services, commercial, industrial, education, administration, health and social services, and others, with percentages of 37.2, 24.4, 15.2, 7.3, 6.8, 5, 3.4, and 0.7, respectively. The work trip destinations extracted from the OD-MRC dataset are used to determine the probability that a functional zone will be the destination of each work type. But considering that the work trip destinations are the TAZs, the possibilities are obtained that specify how likely each TAZ can be a destination for a work type. Thus, a workplace is assigned to an EV user as follows. Firstly, the user's work type is randomly selected based on the work type percentages. Secondly, a TAZ is stochastically selected regarding the TAZs destination probabilities corresponding to the assigned work type. Finally, functional zones corresponding to the work type in selected TAZ are identified, and a random point from the non-home points in the specified functional zones is assigned to the user as the workplace.

(3) Education location

To each EV user that makes a trip with the purpose of Education, a point from the synthetic points in the education zones is assigned as the education location.

5.3.3. Destination choice model for EV trips to non-fixed activity locations

For an EV trip to a non-fixed activity location, a destination choice is made to select a destination location from the synthesized non-home points in functional zones according to the trip purpose. To this end, a destination choice model is developed in three steps, which are summarized below.

(1) Choice set generation

In the lack of travel data at the functional zones level, the destination choice is made at the TAZ level, with the difference that only TAZs are considered that contain the functional zones related to the trip purpose (activity). Hence, the destination choice model generates a choice set that only includes the TAZs with functional zones corresponding to the trip purpose.

(2) Choice probabilities estimation

It is assumed that the choice probability of each TAZ in the choice set is affected by the attractiveness of the TAZ and the travel time from the origin' TAZ to the TAZ. The choice probabilities of TAZs in a choice set are calculated based on OD matrices, which are generated by the Doubly Constrained Gravity Model (DCGM), considering the effects of travel times between TAZs and the attractiveness of TAZs. The DCGM is formulated as a function of travel time, and OD production and attraction ability for each trip purpose k to obtain the corresponding OD matrix OD^k . The pseudocode of Algorithm 1 shows the developed iterative DCGM algorithm. An exponential deterrence function $F^k(c_{ij}) = e^{-\beta^k c_{ij}}$ is used in the DCGM algorithm where c_{ij} are the average travel times between TAZs. The c_{ij} are the mean of the travel times between 100 assumed points in the TAZs that are estimated based on the SPI model by assuming smooth traffic for

urban streets. Furthermore, the β^k is a negative constant value that is calibrated by the Hyman method.

Algorithm 1. DCGM algorithm

```

1.   for each TAZ  $i$  and purpose  $k$  do
2.      $O_i^k = P_i^k$  and  $D_i^k = A_i^k$ 
3.   end
4.   for each OD pair  $i,j$  do
5.      $t_{ij}^k = O_i^k D_j^k F^k(c_{ij})$ 
6.   end
7.   end
8.   while not converged do
9.     for each TAZ  $i$  do
10.     $f = \frac{P_i^k}{\sum_j t_{ij}^k}$  and  $O_i^k = f \cdot O_i^k$ 
11.    for each TAZ  $j$  do
12.       $t_{ij}^k = f \cdot t_{ij}^k$ 
13.    end
14.   end
15.   for each TAZ  $j$  do
16.     $f = \frac{A_j^k}{\sum_i t_{ij}^k}$  and  $D_j^k = f \cdot D_j^k$ 
17.    for each TAZ  $i$  do
18.       $t_{ij}^k = f \cdot t_{ij}^k$ 
19.    end
20.  end
21. end
22. output:  $t_{ij}^k$ 
```

(3) Stochastic destination choice

The choice probabilities of TAZs in the choice set are calculated by normalizing the number of trips between the origin's TAZ to the other TAZs in the choice set that are extracted from OD^k . Accordingly, a TAZ is selected stochastically by comparing a uniform random number of U (0–1) with the cumulative choice probabilities. Then, the functional zone corresponding to the trip purpose is identified in the selected TAZ, and a destination location is randomly selected from the non-home points in the chosen functional zone. Note that if there is more than one functional zone related to the trip purpose in the selected TAZ, one of the functional zones is chosen randomly.

5.4. Driving sub-trajectory

The driving sub-trajectory describes the spatial-temporal characteristics of EV driving on a trip route from the trip's origin to the selected destination location, as well as the profiles of driving speed, EV energy consumption, and SoC. The driving sub-trajectory is simulated in the optimal trip route planning framework.

5.4.1. Optimal trip route planning model

In contrast to traditional trip routing approaches, which typically identify the trip route based on the shortest or fastest path between OD locations, this paper introduces an optimal route planning model specifically designed for EV users. Due to the range anxiety of EV users, this model aims to find the trip route with minimum energy consumption. As such, the proposed optimal trip route planning model utilizes a segment-based EV energy consumption model to identify the route with the minimum energy consumption for each EV trip.

5.4.1.1. EV energy consumption model.

The EV dynamical model can be

Table 1
SPI values for traffic conditions.

Traffic level	SPI	Traffic condition
1	[0, 0.25]	Traffic jam
2	(0.25, 0.5]	Heavy traffic
3	(0.5, 0.75]	Moderate traffic
4	(0.75, 1)	Smooth traffic
5	1	No traffic

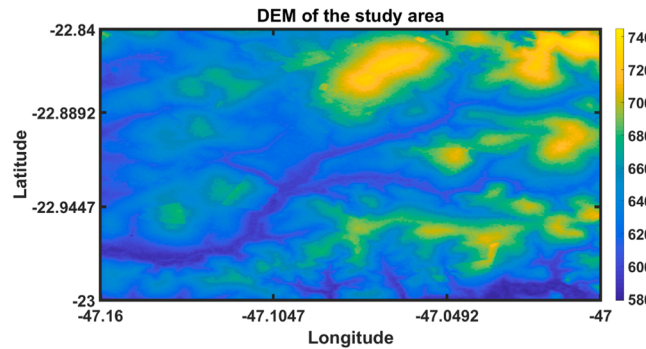


Fig. 10. DEM of the study area.

generally written as follows:

$$m \frac{dv(t)}{dt} = F_{rr}(t) + F_{ad}(t) + F_{hc}(t) \quad (1)$$

Where m is the EV mass (sum of the EV's curb mass (m_{EV}) and the extra load carried by the EV (m_e)), $v(t)$ is the EV driving speed, F_{rr} is the rolling resistance force, F_{ad} is the aerodynamic drag force, and F_{hc} is the hill-climbing force.

Since the time-variant speed profile data of EV driving is not available, the acceleration/deceleration of EV driving is neglected and the time-variant speed $v(t)$ is replaced with the constant average speed \bar{v} . The \bar{v} is estimated based on the Speed Performance Index (SPI) (He et al., 2016), which is the ratio between average driving speed and maximum permissible speed (V_{max}) on a street segment for different traffic conditions. Table 1 shows the SPI values for the traffic conditions.

The V_{max} for a street segment refers to its defined speed limit, which is specified according to the segment's street type. Hence, based on the speed limits of urban streets in the study area, the V_{max} (in km/h) for OSM streets, including motorway, trunk, primary, secondary, tertiary, residential, and service road types, are set to 100, 80, 60, 50, 40, 30, and

15, respectively. Moreover, the V_{max} of motorway-link, trunk-link, primary-link, secondary-link, and tertiary-link street types are 45, 40, 30, 25, and 20, respectively.

Therefore, to estimate \bar{v} for a street segment, first, the traffic condition of the street segment is determined according to the day's traffic time-step and the arrival time of the EV to the segment. Then an SPI value (r_{SPI}) is extracted randomly from the SPI ranges shown in Table 1 according to the determined traffic condition. Finally, \bar{v} is calculated by Eq. (2) based on the extracted r_{SPI} and the V_{max} corresponding to the street type of the segment.

$$\bar{v} = r_{SPI} V_{max} \quad (2)$$

The minimum value of \bar{v} is assumed to be 5 km/h.

The average EV driving time for each street segment is calculated based on the \bar{v} and the length of the street segment, which is calculated by the Haversine formula using the Lat/Long coordinates of street segment nodes.

Therefore, for an EV with mass m , proceeding at a constant \bar{v} on a street segment, the tractive effort is calculated by Eq. (3).

$$F_{tr} = F_{rr} + F_{ad} + F_{hc} = f_r mg + \frac{1}{2} \rho C_d A_f \bar{v}^2 + m g \sin \alpha_s \quad (3)$$

Where f_r is the coefficient of rolling resistance that is calculated by the following equation (Sastry, 2013):

$$f_r = 0.005 + \left(\frac{1}{p} \right) (0.01 + 0.0095(0.001\bar{v})^2) \quad (4)$$

Where p is tire pressure, considered the standard value of 30 bar for EVs. g is the gravitational acceleration, which is equal to 9.81 m/s^2 . ρ is the density of air, C_d is the drag coefficient, and A_f is the frontal cross-sectional area of EV that is calculated by an empirical Eq. (5) (Emam, 2011).

$$A_f = -1.23069 + (0.00011m) + (1.304851BH) - (0.05398((BH)^2)) \quad (5)$$

Where H and B are the height and width of the EV.

α_s is the average slope of the street segment, which is calculated based on the DEM data extracted from the Shuttle Radar Topography Mission (SRTM) (USGS, 2022). Fig. 10 illustrates the one

arc-second DEM data with a resolution of approximately 30 m for the study area.

Calculating the average slope of the urban street segment is described below.

(1) Calculating the slope raster of the study area

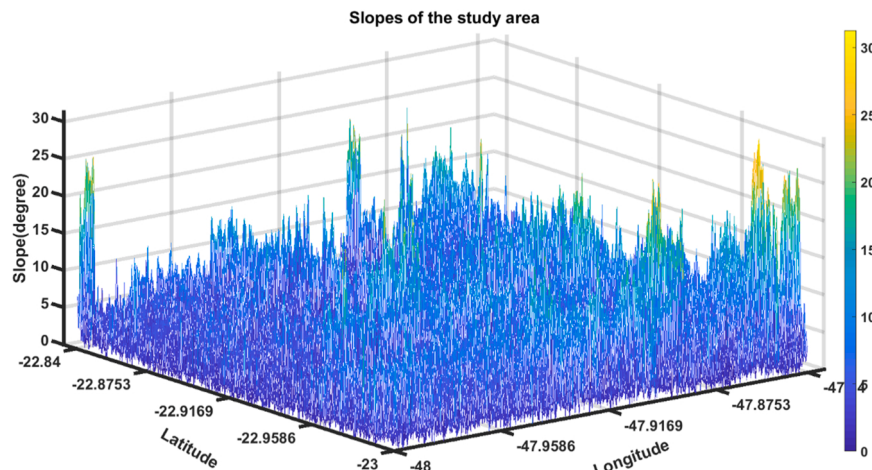


Fig. 11. The slope of the study area.

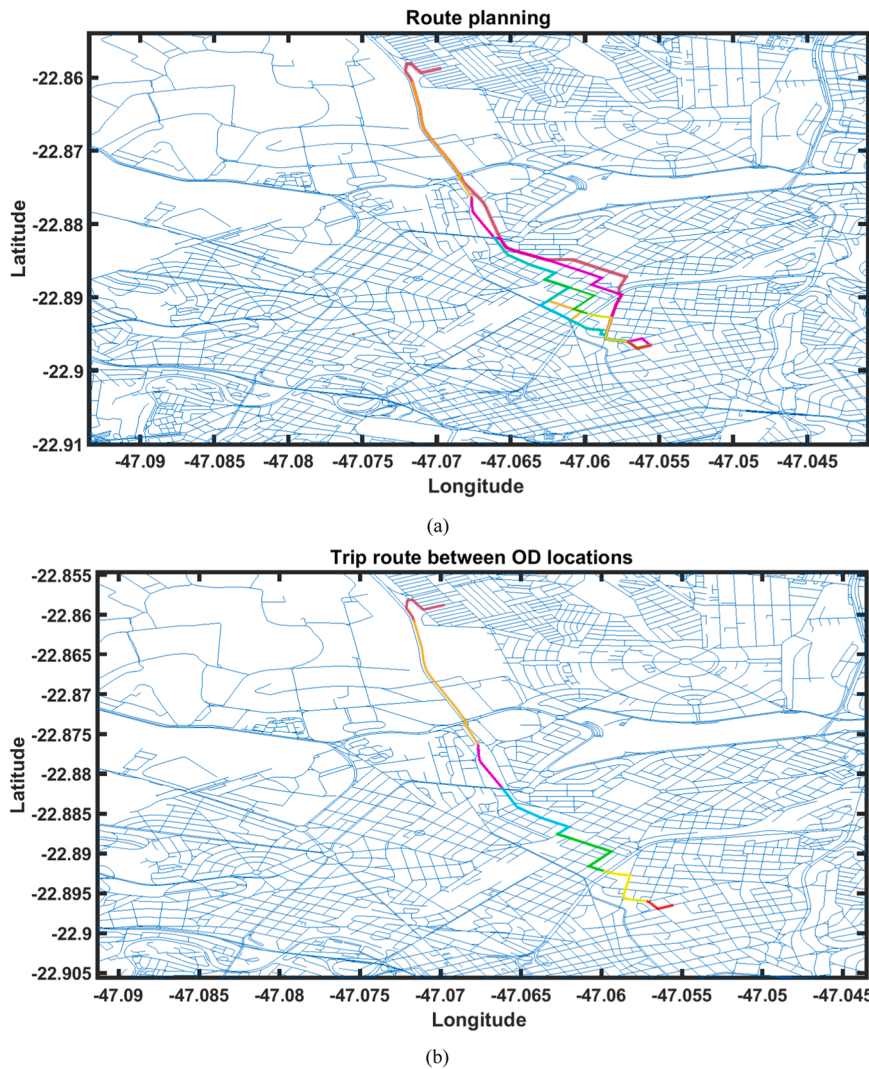


Fig. 12. The dynamic routing between two sample OD locations. (a) pre-route replanning and six en-route (b) final trip route.

The SRTM-DEM data are comprised of pixels with individual elevation values. The slope of each pixel is defined as the change in elevation per unit distance along the path of steepest ascent or descent from the pixel to one of its eight immediate neighbors, which can be calculated in two types of units, degrees or percent. The rates of change of the surface in horizontal (dz/dx) and vertical (dz/dy) directions from the pixel determine the slope that is calculated based on the following equation:

$$\text{slop} = \tan^{-1} \left(\sqrt{[dz/dx]^2 + [dz/dy]^2} \right) \times \frac{180}{\pi} \quad (\text{degree}) \quad (6)$$

For the elevation raster of the SRTM-DEM data of the study area, the slope raster (in degree) for the study area is shown in Fig. 11.

(2) Overlapping the street network and the slope raster

Since the pixels of the slope raster and street segments are specified by Lat/Long coordinates, street segments are overlaid on pixels to identify their intersections.

(3) Calculating the slope of street segments

The slope value of a street segment is the average slope of all intersecting pixels with that street segment.

Therefore, the mechanical power consumption at wheels is calculated by Eq. (7).

$$P_m = F_n \bar{v} = \left(f_r mg + \frac{1}{2} \rho C_d A_f \bar{v}^2 + m g \sin \alpha_s \right) \bar{v} \quad (7)$$

The energy losses that occur in different components of the electric powertrain are described by the efficiencies, which include efficiencies of battery, power converter, e-motor (electric motor and control system), and mechanical powertrain, denoted by η_{bat} , η_{conv} , η_{em} , η_{mp} , respectively. Thus, the overall propulsion power balance equation can be written as the following equations.

$$(P_{bat} - P_a) \eta_{bat} \eta_{conv} \eta_{em} \eta_{mp} = P_m \quad (8)$$

$$P_{bat} = \frac{P_m}{\eta_{bat} \eta_{conv} \eta_{em} \eta_{mp}} + P_a \quad (9)$$

Where, P_a is the accessories power consumed by lights, air conditioning, etc.

Considering the length of the segment l_s , which is calculated by the Haversine formula, and the driving time on the segment (t_s), the total consumed energy of the EV's battery on the i^{th} segment (E_s^i) is calculated as below.

$$E_s^i = P_{bat} \cdot t_s \quad (10)$$

For an EV trip, the total energy consumption of EV driving on the trip route is obtained as

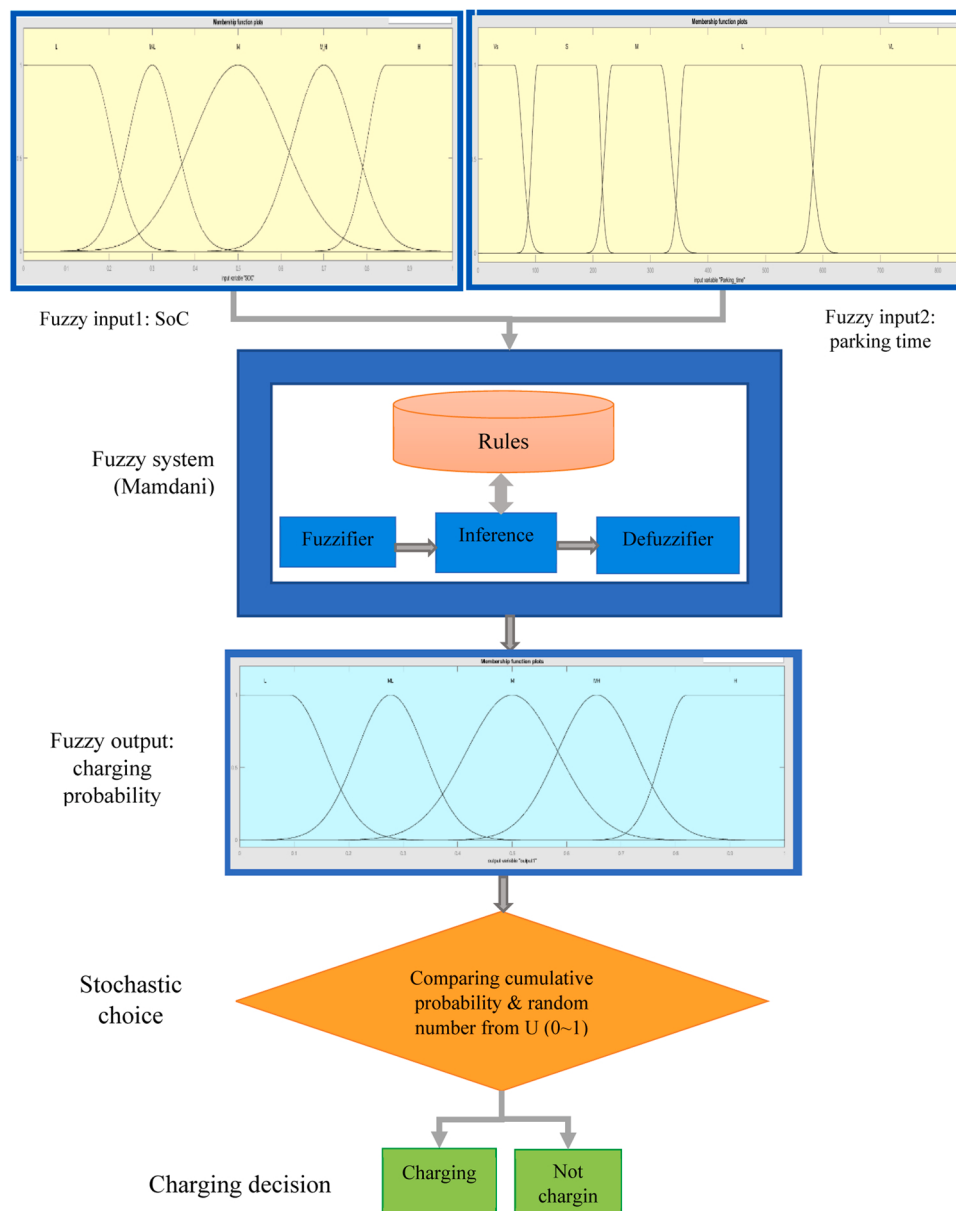


Fig. 13. The stochastic charging decision by Fuzzy system.

$$E_t = \sum_{i=1}^{N_s} E_s^i \quad (11)$$

Where N_s is the number of the trip route's segments. Consequently, the arrival SoC of the EV at the destination location (SoC^{ar}) is calculated by the following equation.

$$SoC^{ar} = SoC^d - \frac{E_t}{B_{EV}} \quad (12)$$

Where SoC^d is the SoC of the EV at the departure of the trip's origin location at the initial moment of driving and B_{EV} is the capacity of the EV's battery.

5.4.1.2. Dynamic minimum-energy trip route planning. The minimum-energy route planning model finds the path with minimum energy consumption of EV driving between each pair of graph nodes as follows. Firstly, the traffic simulation determines the traffic condition of all OSM street segments regarding the traffic time-step and time of route

planning. Then, the segment-based energy consumption model calculates the energy consumption of EV driving on the street segments based on the driving speed, driving time, etc. Finally, each edge (street segment) of the street network graph is assigned a weight that indicates the EV driving energy consumption on that edge, and Dijkstra finds the minimum-energy trip route on the weighted graph.

Due to the changes in street traffic conditions during EV driving on urban streets, the driving sub-trajectory is simulated via the dynamic minimum-energy trip route planning model, which consists of one pre-trip route planning at the departure time of the origin and several en-route replanning during the driving in response to the changes in the street segments' traffic conditions. The driving sub-trajectory simulation is summarized as follows. At the departure time of origin, the pre-trip route planning finds the initial minimum-energy trip route from the origin to the destination. After departing the origin, while the driving on the initial route is modeled segment-by-segment, the possibility of en-route replanning is checked at each intersection node by considering traffic's time-step changes. If the time-step has changed when the EV reaches an intersection node, the route is updated by the en-route

replanning from the intersection node to the destination location. This process is repeated during driving on the updated trip routes until the EV reaches the destination. Fig. 12 shows the dynamic minimum-energy trip route planning process for a trip between sample OD locations in two functional zones.

Therefore, the driving sub-trajectory of the j th trip of an EV that describes the spatial-temporal characteristics, speed profile, energy consumptions, and SoC profile of EV driving on the final minimum-energy trip route between OD locations is expressed as follows:

- Spatial-temporal features of driving (ST_Dr^j)

$$ST_Dr^j = \{(lat_1^j, lon_1^j, t_1^j), (lat_2^j, lon_2^j, t_2^j), \dots, (lat_n^j, lon_n^j, t_n^j)\} \quad (13)$$

Where (lat_1^j, lon_1^j) , (lat_n^j, lon_n^j) indicate the Lat/Longs of OD locations, and t_1^j and t_n^j are the departure time from the origin and arrival time at the destination. (lat_2^j, lon_2^j) to $(lat_{n-1}^j, lon_{n-1}^j)$ indicate the Lat/Longs of the trip route's street intersections, and t_2^j to t_{n-1}^j demonstrate the times to reach or leave these intersections.

- Average driving speed and driving time profile (vt_Dr^j)

$$vt_Dr^j = \{(v_1, t_1), (v_2, t_2), \dots, (v_n, t_n)\} \quad (14)$$

Where v_1 to v_n and t_1 to t_n are the average velocity and time of EV driving on the trip route's segments 1 to n , respectively.

- EV energy consumption profile (E_Dr^j)

$$E_Dr^j = [e_1, e_2, \dots, e_n] \quad (15)$$

Where e_1 to e_n are the energy consumption of EV driving on the street segment 1 to n .

- SoC profile (SoC_Dr^j)

According to the D_E^l and EV's battery capacity, the SoC profile for the j th trip is calculated as:

$$SoC_Dr^j = [SoC_1^j, SoC_2^j, \dots, SoC_n^j] \quad (16)$$

Where SoC_1^j is the SoC at the departure time of the origin location, SoC_n^j is the arrival SoC (SoC^{ar}) at the destination location, SoC_2^j to SoC_{n-1}^j are the SoCs at the trip route's intersections.

5.5. Charging sub-trajectory

As the objective of charging sub-trajectory modeling is to predict the time, location, and quantity of slow and fast charging demands across the urban area, it is assumed that at each destination, there are enough slow/ fast charging facilities to charge all arriving EVs.

Once the user arrives at the destination, he/she decides whether to charge the EV. The EV user's charging decision at a destination is modeled by considering the main affecting factors, including the SoC^{ar} , the EV user's mileage anxiety, required SoC for the next trip ($SoC_{n.t}$) and parking time (t_p).

Due to mileage anxiety, it is assumed that EV users prefer to charge the EV before the battery's SoC reaches a certain SoC level, even if EV has enough energy to meet the next trip. Hence, EV user's mileage anxiety is quantified by a minimum SoC (SoC_{min}), which user prefers to keep the SoC of the EV more than it. Thus, an EV user decides to charge his/her EV when the SoC^{ar} is lower than the sum of SoC_{min} and $SoC_{n.t}$.

Furthermore, the user may decide to charge the EV at the destination regardless of the concern about range anxiety and the required energy for the next trip. To simulate this user's decision-making process, a Fuzzy system is developed, whose inputs are SoC^{ar} , and t_p , and its output is the charging probability. With several trials and practices, the

Gaussian shapes are chosen for both input and output membership functions. The five SoC levels (low, medium-low, medium, medium-high, and high), five parking times (very short, short, medium, long, and very long), and five charging probabilities (low, medium-low, medium, medium-high, and high) are considered to define the fuzzy inputs and outputs variables. EV user charging decision (i.e., charging or not charging) is determined stochastically based on obtained charging probability. Fig. 13 shows the stochastic charging decision model based on the Fuzzy system.

Once the charging decision is made, the EV user must choose the charging mode that is divided into slow and fast charging. Slow charging is preferred due to battery life, charging price, etc. However, the fast charging mode will be chosen if the parking time is very short (e.g., less than 30 minutes) or if slow charging within the parking time cannot meet the minimum expected SoC (SoC_{min}^{exp}) of the EV user, which is calculated as follows:

$$SOC_{min}^{exp} = (SOC_{n.t} + SOC_{min}) - SOC^{ar} \quad (17)$$

Hence, if Eq. (18) is satisfied or if t_p is less than 30 minutes, the user chooses to charge the EV by fast charging power, otherwise, the slow mode is selected.

$$\frac{\eta P_{slow} t_p}{B_c} + SOC^{ar} < SOC_{min}^{exp} \quad (18)$$

Where P_{slow} is the slow charging mode, η is the charging efficiency and B_c is the battery capacity. When the EV user has chosen the charging mode, the EV's charging demand and charging time are calculated.

In the slow charging, by considering the parking time and charging power rate, the EV can be fully charged if the parking time is more than the required time for SoC^{ar} to reach SoC_{max} , otherwise, the charging time is equal to the parking time. Moreover, the EV is assumed to be fully charged in fast charging mode. So, the user extends the parking time if the parking time is less than the required time to charge fully.

The previous descriptions for charging mode decision and demand calculation are summarized in the following two equations:

$$\text{Slow charging : } \begin{cases} \frac{\eta_s P_s t_p}{B_c} + SOC^{ar} > SOC_{min}^{exp} \\ t_{fch_s} = \frac{(SoC_{max} - SOC^{ar}) B_c}{\eta_s P_s} \\ t_{ch_s} = \begin{cases} t_{fch_s} & t_{fch_s} \leq t_p \\ t_p & t_{fch_s} \geq t_p \end{cases} \\ D_s = \begin{cases} P_s t_{fch_s} & t_{fch_s} \leq t_p \\ P_s t_p & t_{fch_s} \geq t_p \end{cases} \end{cases} \quad (19)$$

$$\text{Fast charging : } \begin{cases} \frac{\eta_f P_{slow} t_p}{B_c} + SOC^{ar} < SOC_{min}^{exp} \\ t_{fch_f} = \frac{(SoC_{max} - SOC^{ar}) B_c}{\eta_f P_{fast}} \\ t_{ch_f} = \begin{cases} t_{fch_f} & t_{fch_f} \leq t_p \\ t_p + (t_{fch_f} - t_p) t_{fch_f} & t_{fch_f} \geq t_p \end{cases} \\ D_f = P_f t_{fch_f} \end{cases} \quad (20)$$

Where P is the charging power rate, η is the charging efficiency, t_{fch} is the time for full charging, and D is the charging demand. The subscripts s and f refer to slow and fast charging modes.

At the departure time from the destination location, the departure SoC of EV (SoC^d) is updated based on Eq. (21) and Eq. (22) for slow and fast charging, respectively.

$$SoC^d = SOC^{ar} + (D_s / B_c) \quad (21)$$

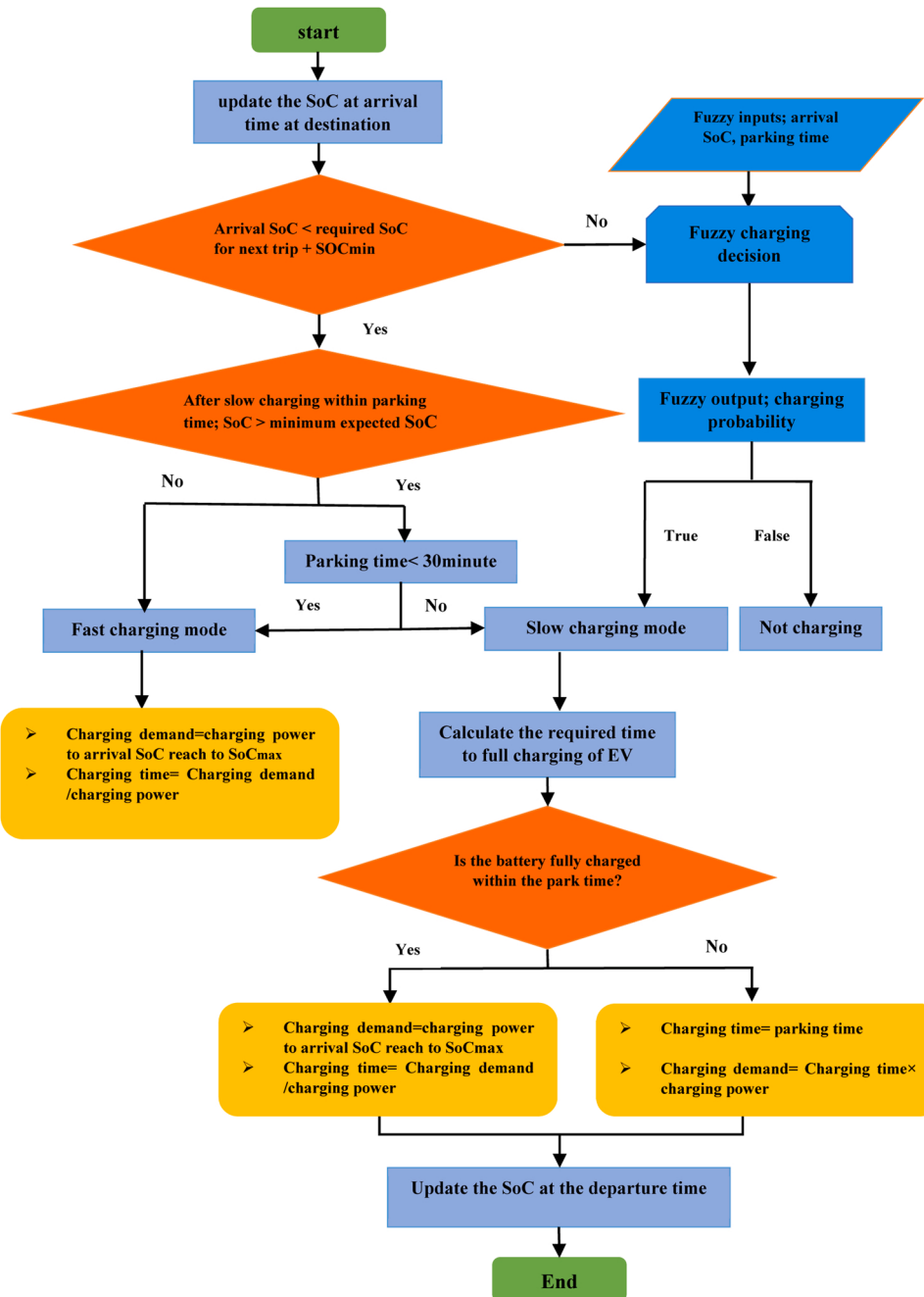


Fig. 14. Flowchart of charging sub-trajectory simulation.

Table 2
Probability distribution functions of parking time.

Travel activity	PDF	Parking time
Home linger	Gamma	$\Gamma(1.2981, 138.3170)$
Work	Gaussian Mixture Distribution	$GMD : \begin{cases} p = [0.684610.31539] \\ \mu = [594.428255.3] \\ \sigma = [159.128120.87] \end{cases}$
Education	Weibull	$W(360.0618, 2.4768)$
Shopping	Lognormal	$L(3.866, 0.8744)$
Meal	Lognormal	$L(3.9178, 0.5743)$
Health	Loglogistic	$L(4.5577, 0.4828)$
Recreation	Gamma	$\Gamma(1.7884, 102.8747)$
Others	Weibull	$W(64.4109, 0.6585)$

$$SoC^d = SoC^{ar} + \left(\frac{D_f}{B_c} \right) = SoC_{\max} \quad (22)$$

Therefore, for the j th trip of an EV, the charging sub-trajectory (CTR^j), including the charging location (l_c), charging start time (t_{cs}), slow charging load demand (D_s) or fast charging load demand (D_f), and the charging duration (t_c) is expressed as below.

$$CTR^j = \{(lat_{ch}^j, lon_{ch}^j, t_{cs}^j, D^j, t_c^j\} \quad (23)$$

Fig. 14 shows the flowchart of the charging sub-trajectory simulation.

5.6. Parking sub-trajectory

The parking times at different activity locations (destination types)

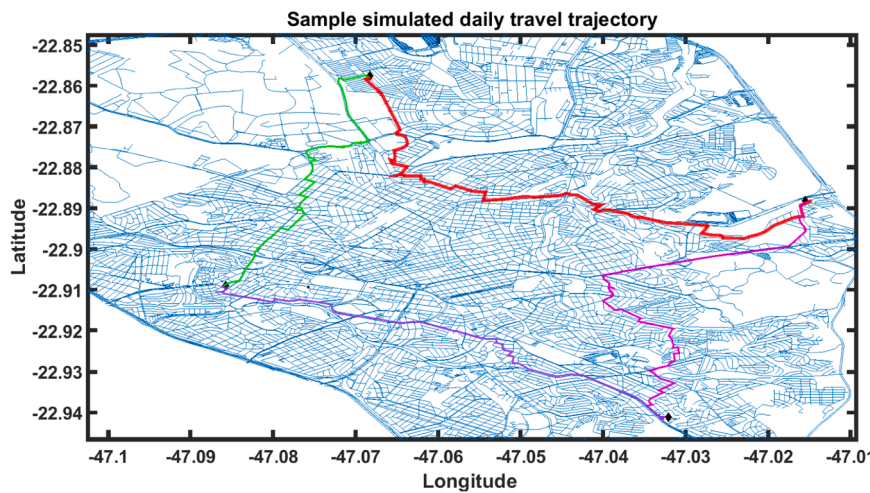


Fig. 15. Trip routes of a sample simulated daily travel trajectory in the study area.

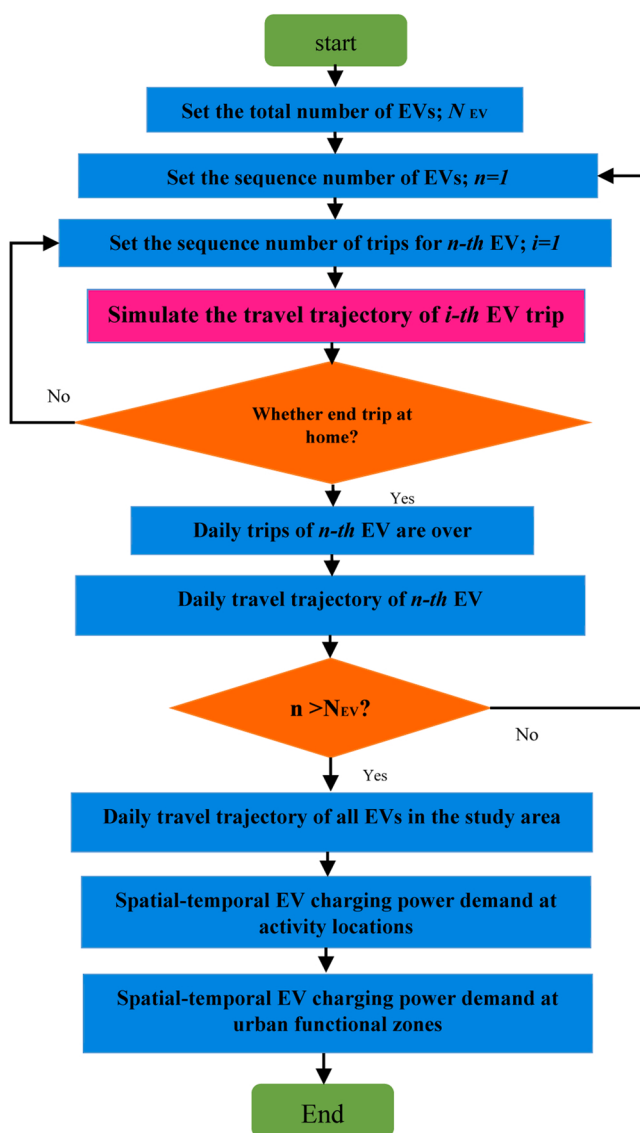


Fig. 16. Flowchart of spatial-temporal charging load prediction.

are modeled by PDFs calibrated by dwelling times at different

destination types extracted from the OD-MRC dataset. Table 2 presents the parameters of the PDFs used to describe the parking duration at various destination types. These PDFs are truncated from low tail to five minutes to prevent the generation of zero or negative random numbers.

If the user decides not to charge the EV, it is parked at a non-EV parking location at the destination for a specific parking time extracted from the PDF corresponding to the destination type. Thus, for the j th trip of an EV, the parking sub-trajectory (PTr^j), specified by the Lat/Longs of the destination location and the parking time, is described below.

$$PTr^j = \left\{ \left(lat_p^j, lon_p^j \right), t_p^j \right\} \quad (24)$$

Therefore, the j th trip of an EV is simulated by a travel trajectory, including the two sub-trajectories of DTr^j and PTr^j or CTr^j .

6. Forecasting the spatial-temporal distribution of urban charging load

The spatial-temporal charging load at different destinations and functional zones of the urban area is predicted based on the stimulated daily travel trajectories of the EVs in the urban area.

6.1. EV's Daily travel trajectory

The EV's daily travel trajectory is constructed by merging the travel trajectories of its individual trips that are simulated in a multi-location and multi-purpose framework. The steps of the daily travel trajectory simulation are as follows.

- (1) For the first EV trip, which starts from home, a departure time is decided randomly from the PDF of the first departure time from home.
- (2) The trip purpose of the first trip is obtained stochastically from hourly TPM corresponding to the hour of departure from home.
- (3) The travel trajectory of the trip is simulated by two sub-trajectories of three sub-trajectories of driving, charging, and parking.
- (4) For the second and further trips, the departure time is calculated as the sum of arrival and parking times at the destination. Moreover, the trip purpose is determined stochastically based on hourly TPM regarding departure time and the activity type of the trip's origin.

Table 3
Electric vehicle specifications.

EV model	Selling percentages (%)	EV specification				
		Curb mass (kg)	Width(mm)	Height(mm)	Drag coefficient	Battery capacity
AUDI E-TRON	21.3	2490	1935	1629	0.28	71
CHEVROLET BOLT	12.6	1616	1765	1595	0.308	60
Nissan Leaf	12.3	1558	1791	1560	0.28	40
JAGUAR I-PACE	11.5	2140	1895	1565	0.29	90
BMW i3	9.5	1245	1775	1598	0.29	33.2
RENAULT KANGOO Z. E	7.5	1530	1829	1801	0.29	33
JAC IEV40	7.3	1460	1750	1560	0.35	40
RENAULT ZOE	3.84	1500	1703	1562	0.29	45
JAC IEV 20	3.38	1340	1685	1570	0.35	41
MERCEDES-BENZ EQC	3.15	2495	1884	1624	0.26	80
BYD ET3	2.2	2420	1772	1875	0.28	50.3
TESLA MODEL 3	1.3	1611	1849	1443	0.23	53
TESLA MODEL Y	1.3	2003	1921	1624	0.23	74
TESLA MODEL X	0.95	2352	1999	1676	0.25	75
PORSCHE TAYCAN 4 s	0.6	2140	1966	1379	0.22	71
TESLA MODEL S	0.58	2027	1963	1445	0.24	75
JAC IEV 330 P	0.25	2200	1880	1830	0.35	67.2
RENAULT TWIZY	0.23	450	1234	1454	0.64	6.1
BYD E5	0.11	1845	1765	1500	0.28	47
JAC IEV 60	0.11	1665	1782	1656	0.35	63

Table 4
EV's efficiencies.

	Efficiency (%)	
	Min.	Max.
η_{bat}	93	99
η_{conv}	90	98
η_{em}	85	96
η_{mp}	87	93

- (5) If the trip purpose is “end trip,” the trip will be the last one, the travel trajectory for the last trip is simulated, and the daily travel of the EV is over.
- (6) If the trip purpose is not the “end trip”, the daily travel of the EV will continue, and the process will be repeated from step (3).
- (7) The daily travel trajectory of the EV is obtained by combining the simulated travel trajectories of daily trips based on steps (1)-(6), which can consist of two or more trips with different purposes.

Fig. 15 shows the trip routes of the daily travel trajectory for a home-to-home tour with four trips.

6.2. Spatial-temporal EV charging load at urban locations and functional zones

The total charging load $P_l(t)$ at time t for a location l is calculated by the following equation:

$$P_l(t) = \sum_{m=1}^M p_l \quad (25)$$

Where M is the number of EVs that are charged simultaneously at time t at destination location l , p_l is the charging power rate of the charging piles at location l . Accordingly, the total charging power $P_z(t)$ of the urban functional zone z at time t is the sum of the charging power of locations in the zone that is calculated as:

$$P_z(t) = \sum_{l=1}^{nl} P_l(t) \quad (26)$$

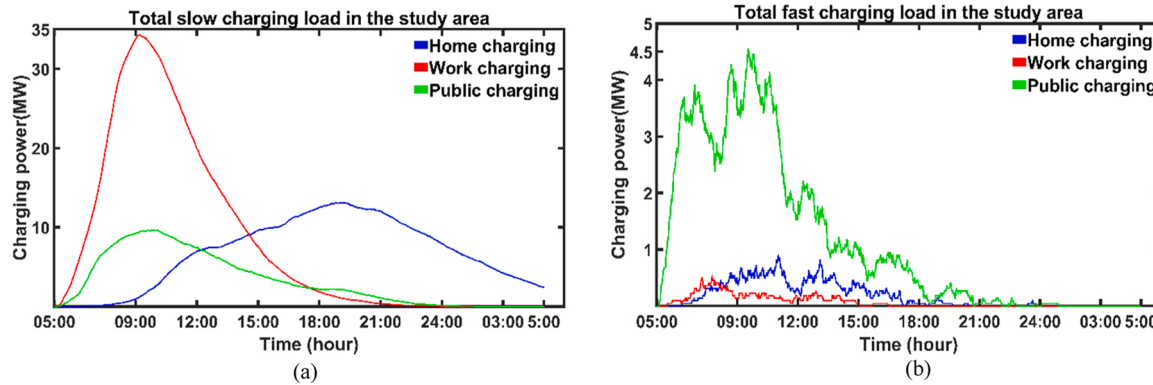


Fig. 17. Total charging load of the study area for a typical day. (a) slow charging load profile, (b) fast charging load profile.

Table 5
Daily charging demand of different destination types.

destination type	Home (H1)	Home (H2)	Work	Education	Shopping	Public Meal	Health	Recreation	Others
Slow charging load (kWh)	6739.5	159333	200488	31541	2988	289.1	6409	8291	27939
Fast charging load (kWh)	4088	-	1693	973.5	3600	1701	2176	1222	17315

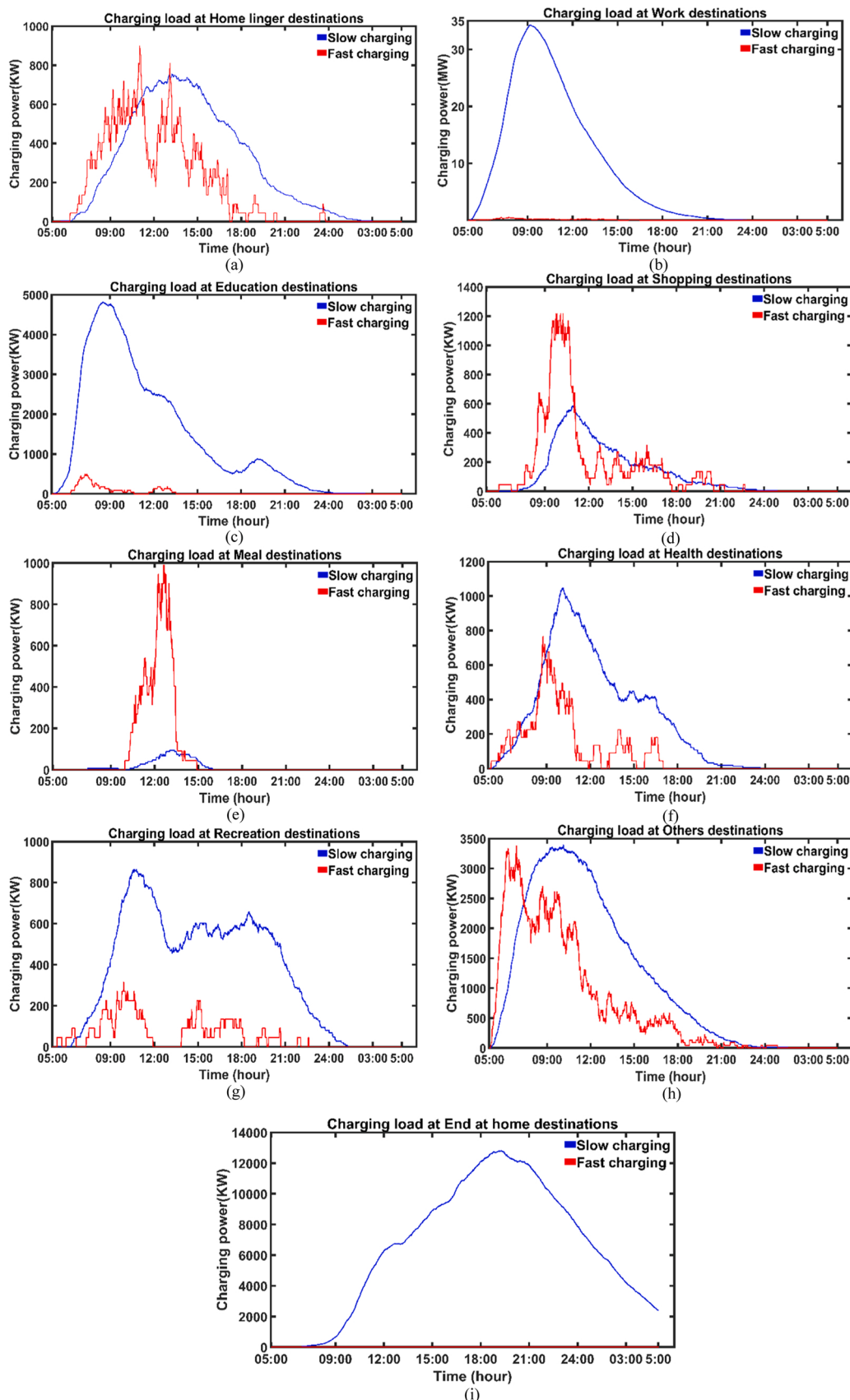


Fig. 18. Charging load profiles of destination types for a typical weekday. (a) Home lingers, (b) Work, (c) Education, (d) Shopping, (e) Meal(lunch), (f) Health, (g) Recreation, (h) Others, (i) End at home.

Table 6
Daily charging demand (kWh) of functional zones.

	Home		Work		Public	
Functional zones	Slow	Fast	Slow	Fast	Slow	Fast
Residential	83482	1898	47209	277	82.5	1640
Commercial and service	1726	42	40322	258	14254	10032
Industrial	-	-	39186	519	-	-
Social and service	-	-	7549	65.25	48600	6772
Mixed zones	80864	2148	66223	573.75	14522	8351

Where nl is the number of locations in the zone.

The flowchart of the spatial-temporal charging load prediction method is shown in Fig. 16.

7. Simulation results and analysis

This section presents the simulation results of applying the proposed simulation method for forecasting the spatial-temporal distribution of charging demand in the urban area of Campinas, Brazil.

7.1. Simulation parameter assumptions

Although the majority of models in this paper are developed based on the actual data from the study area, several parameters related to the EV are assumed because the EV is not populated yet in the study area. These assumed simulation parameters are:

(1) EV's number

The number of EVs in the urban area is determined based on an assumed EV penetration rate and the number of private cars in Campinas reported by the Brazilian Ministry of Infrastructure (Infraestrutura, 2022). Based on the number of private cars, which is 619,448, and the city area of 795.667 km^2 , the car per area (car/km^2) is 778.5267. Hence, for the study area of 116.525 km^2 , and the assumed EV penetration level of 20%, the estimated number of EVs in the study area is set to 18,144 ($N_{EV} = 18,144$).

(2) EV's specifications

The EV specifications used in the EV energy consumption model are adapted from the best-selling EV brands in Brazil (Automotive, 2022) and EV specifications datasets (EVspecifications, 2022). Table 3 illustrates the selling percentages of these EV brands and their specifications, including curb mass (m_{EV}), EV width (B) and height (H), drag coefficient (C_d), and battery capacity (B_{EV}). Accordingly, a brand is randomly assigned to each EV in the study area based on the selling percentages, and the brand specifications are used as the EV specifications in the corresponding simulations.

In addition to these specifications, the extra load carried by the EV (m_e) and the accessories power (P_a) are modeled with Normal distributions $N(100 \text{ kg}, 20)$ and $N(500 \text{ W}, 25)$, respectively.

(3) The efficiencies of EV components

According to (Faria et al., 2012), the efficiencies of each EV (i.e., η_{bat} , η_{conv} , η_{em} , η_{mp}) are assumed as constant values, chosen as random numbers between the corresponding minimum and maximum efficiencies of Table 4.

(4) Mileage anxiety

It is assumed that SoC_{min} , which is caused by the EV user's mileage anxiety, obeys the Normal distribution ($N(\mu=0.466, \sigma=0.179)$) (Yi et al., 2019), which is truncated from the lower tail to 0.2 and from the upper tail to 0.8.

(5) Initial SoC

The initial SoC (i.e., the SoC of EV at the first departure time of home) of each EV is extracted randomly from the Normal PDF, $N(0.5, 0.1)$ (Ghotge et al., 2021), which is truncated to 0.35 and 0.9 from the upper and lower tails, respectively.

(6) Maximum SoC(SoC_{max})

The SoC_{max} , which is considered the maximum SoC of EV charging at a destination location, is set to 0.8 and 0.9 for slow and fast charging, respectively.

(7) Charging power rate of chargers

The slow charging power in the home is assumed to be 3.3 kW, whereas it is considered 6.7 kW in other activity locations. The fast-charging power rate is set to 45 kW. Moreover, the charging efficiencies of chargers are assumed to be a random number between 0.8 and 0.9.

(8) Simulation time-step

The simulation adopts a one-minute interval to model EV charging power demand. Consequently, the prediction of slow and fast charging loads at destinations and urban functional zones is conducted with a one-minute time step.

7.2. Total charging power demand of the study area

From the total urban charging demand, the share of charging loads at home, work, and the public are 35.68%, 42.4%, and 21.92%, respectively. 97.6% of the home charging demand is slow, and 2.4% is fast. 99.16% and 0.84% of work charging demands are slow and fast, respectively. For public charging locations, 74.16% of total demand is slow charging, and 25.84% is fast. Fig. 17 shows the total slow and fast charging power demand profiles at home, work, and public, for a typical weekday from 5:00–5:00 of the next day. The public charging demand is the sum of charging demands at the destination types, including Education, Shopping, Meal(lunch), Health, Recreation, and Others.

As seen from Fig. 17, the slow charging demand mainly includes morning charging at work and nighttime charging at home due to the convenience of charging and long parking times at workplaces and homes. Most EV users in the simulation are employed users (i.e., 56.8% of EV users) who prefer to charge EVs at workplaces during work time. Moreover, nighttime charging at home is more favorable for EV users because of low price energy and long night parking time at home.

7.3. Charging power demands at destination types

Table 5 shows the daily slow and fast charging demand amounts (in kWh) of the different destination types in the study area.

Fig. 18 (a) to Fig. 18 (i) show the slow and fast charging power load profiles for destination types.

Fig. 18(a) shows the charging demand of H_1 that concentrates at midday when a number of EV users return home for lunch and rest. Due to the short parking time of EVs at H_1 , some EVs have fast charging demands.

As can be seen from Fig. 18(b), the charging demand at Work is mostly slow charging due to the long parking time of EVs at workplaces. Since most EVs reach the workplace between 7:00–9:00, the charging power demand increases quickly and peaks around 09:15. After that, the charging load demand decreases gradually as the EVs leave the workplaces.

Fig. 18 (c) shows the charging demand profile of Education destinations, which are the destinations of 12.9% of EV users for regular education (e.g., university) and non-regular education (e.g., language institute). This charging demand profile has a peak in the morning mainly due to regular education and a small peak at 19:00. At these destination locations, fast charging demand is lower than slow charging demand due to the relatively longer parking time.

As shown in Fig. 18(d), the fast charging demand in Shopping

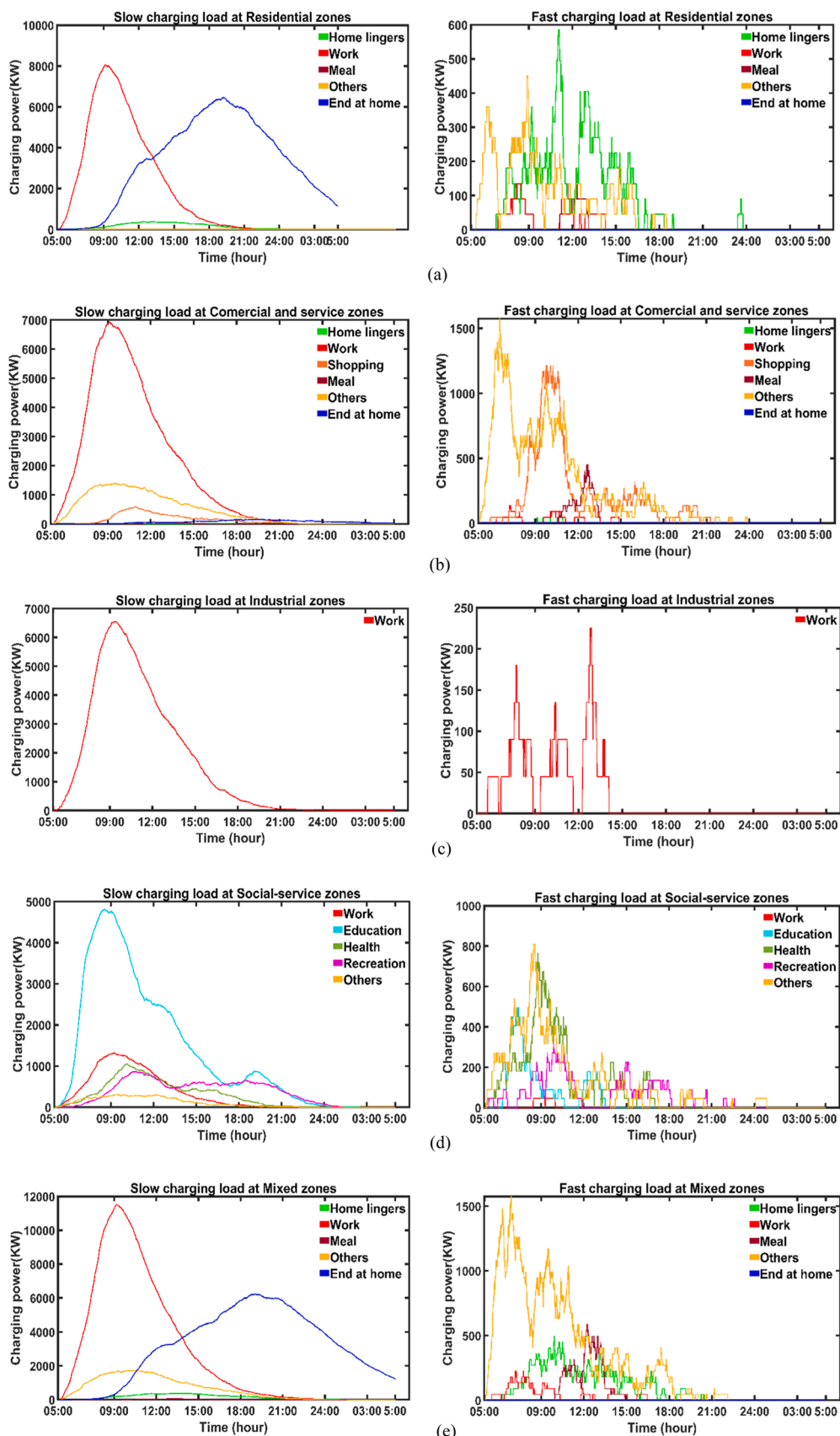


Fig. 19. Daily slow charging demand profiles at functional zones. (a) slow/fast charging at residential zones, (b) slow/fast charging at commercial and service, (c) slow/fast charging at industrial zones, (d) slow/fast charging at social-service zones, (e) slow/fast charging at mixed zones.

destinations is higher than the slow one due to the short EV parking time. According to Fig. 18(e), almost all charging power demand in the Meal (lunch) is fast charging and concentrated between 11:00–15:00, corresponding to lunchtime.

Fig. 18 (f) shows that the slow charging demand profile of the Health peaks at midday, and it is more frequent than the fast one. Fig. 18 (g) shows Recreation destinations' charging power demand profile, which is essentially low on weekdays. Due to the relatively long parking time, the slow charging demand is higher than the fast charging demand.

As seen from Fig. 18 (h), the charging demand trend of 'Others' destinations is similar to Work, increasing at first and then decreasing, with no charging load demands between 24:00 and 5:00 the next day. Since EV parking time in 'Others' destinations is relatively short on weekdays, especially in the morning, fast charging demand is high in the morning, and slow charging demand is higher at other times.

Fig. 18 (i) shows the charging power demand profile at H_2 . It is different from H_1 and consists of entirely slow charging that is low between 5:00 and 10:00 and increases after 10:00. As the number of EV users increases at home after returning from work, slow charging demand increases rapidly, reaching a peak at 19:30 and then decreasing gradually until 5:00 on the next day.

7.4. Charging power demands of urban functional zones

The charging demand of a functional zone is the sum of the charging demands of the charging locations in the zone. Table 6 shows the charging demand amounts of home, work, and the public at different functional zones.

Fig. 19 (a) to Fig. 19 (j) show the slow and fast charging power demand profiles of urban functional zones.

As seen in Fig. 19 (a), the charging demand in residential zones is almost entirely slow charging at home and work. Home charging demand includes midday charging demand at H_1 and night charging at H_2 . In addition, the fast charging demand of residential zones is mainly due to EV charging at Meal and Others. As such, in addition to the slow charging piles at homes, the FCSs can be installed in residential zones to meet the fast charging demand of EV users.

Fig. 19 (b) shows that most of the slow charging demand in the commercial and service functional zones group is due to daytime charging at workplaces during work times and nighttime charging at homes. Moreover, these functional zones have a significant fast charging demand for public destinations (mainly city center area and shopping malls), which makes these zones good candidates for installing fast charging infrastructures.

According to Fig. 19 (c), the charging demand at industrial zones is totally slow charging demand during work time between 9:00–18:00. The slow charging demand is much higher than the fast one because of the long parking time of EVs at industrial workplaces. As such, industrial workplaces require a large number of slow charging piles to meet the charging demand of their workers.

Fig. 19 (d) shows that the slow charging demand in the social-service functional zones is mainly due to the charging in the Education and Health destinations. Furthermore, a large part of fast charging demands at these zones is the charging demands at 'Others' destinations because these zones include diverse activity locations that attract a significant fraction of EV trips with 'Others' destination types.

According to Fig. 19 (e), most of the slow charging demand in the mixed zones is from EV charging during the day in workplaces and overnight at homes. However, the fast charging demand is mainly in the morning at commercial, social, and administrative activity locations.

8. Conclusion

This study presents a novel method for forecasting the spatial-temporal distribution of urban charging loads based on the EV travel trajectory simulation in the integrated framework of the urban street

network and functional zones. To achieve more realistic forecasts of urban charging demands, the EV travel trajectories are simulated based on the real-world data of the study area, including the geospatial data of urban streets and functional zones, traffic data extracted from Google Maps, travel data, demographic data, and DEM data.

The created OSM street network provides opportunities for developing a new tool to extract street traffic conditions from the GMLT and calculate the average slopes of urban streets based on DEM data. The created OSM street network is integrated with urban functional zone polygons to provide a spatial framework for simulating EV user travel behavior by several models, including the stochastic trip purpose prediction model, destination choice model, dynamic trip route choice model, fuzzy charging decision model, and probabilistic models for first departure time from home and parking time. These models are employed to simulate each EV trip through a travel trajectory. By merging the travel trajectories of all trips of an EV user in a day, the daily travel trajectory of the EV is constructed. The daily travel trajectories of the available EVs within the urban area are then utilized to predict the spatial-temporal distributions of slow and fast EV charging power demands across various locations and functional zones within the urban area.

The results of applying the proposed simulation method in the urban area of Campinas, Brazil, show that the highest percentage of urban charging demand is slow charging at home and work. The charging load at home, work, and public are 35.68%, 42.4%, and 21.92% of the total urban charging demands, respectively. For home charging, 97.6% of the total demand is slow charging, and 2.4% is fast. 99.16% and 0.84% of the work charging demand are for slow and fast charging, respectively. 74.16% of total charging demand at public locations is slow, and 25.84% is fast. Furthermore, the share of charging demand to the total urban charging demand at residential, commercial and service, industrial, social and service, and mixed zones are 28.24, 13.98, 8.33, 13.22, and 36.23, respectively.

This study has a few limitations that can be addressed in future studies. Once the study area is populated with EVs and the necessary data on EV travel trajectories becomes available, the proposed method can be validated for its accuracy, and also it can be compared by data-driven methods.

CRediT authorship contribution statement

Ernesto Ruppert Filho: Funding acquisition, Supervision, Writing – review & editing. **Tarcio Andre dos Santos Barros:** Conceptualization, Funding acquisition, Project administration, Supervision, Writing – review & editing. **Eslam Mahmoudi:** Conceptualization, Data curation, Investigation, Methodology, Software, Visualization, Writing – original draft, Writing – review & editing.

Declaration of Competing Interest

The authors declare that they have no known competing financial interests or personal relationships that could have appeared to influence the work reported in this paper.

Data availability

The data that has been used is confidential.

Acknowledgements

This work was supported by the National Council for Scientific and Technological Development, CNPq, Brazil under grants 402983/2021-1, 308589/2022-0.

References

- Abbasi, M.H., Taki, M., Rajabi, A., Li, L., Zhang, J., 2019. Coordinated operation of electric vehicle charging and wind power generation as a virtual power plant: a multi-stage risk constrained approach. *Appl. Energy* 239, 1294–1307. <https://doi.org/10.1016/j.apenergy.2019.01.238>.
- Alfaverh, F., Denaï, M., Sun, Y., 2023. Optimal vehicle-to-grid control for supplementary frequency regulation using deep reinforcement learning. *Electr. Power Syst. Res.* 214 (Part B), 108949. <https://doi.org/10.1016/j.epsr.2022.108949>.
- Al-Obaidi, A., Khani, H., Farag, H.E.Z., Mohamed, M., 2021. Bidirectional smart charging of electric vehicles considering user preferences, peer to peer energy trade, and provision of grid ancillary services. *Int. J. Electr. Power Energy Syst.* 124 (2021), 106353. <https://doi.org/10.1016/j.ijepes.2020.106353>.
- Arias, M.B., Kim, M., Bae, S., 2017. Prediction of electric vehicle charging-power demand in realistic urban traffic networks. *Appl. Energy* 195, 738–753. <https://doi.org/10.1016/j.apenergy.2017.02.021>.
- Automotive, 2022. Carros elétricos mais vendidos do Brasil. (<https://automotivebusiness.com.br/pt/posts/setor/>) - automotivo/carros-eletricos-mais-vendidos-brasil/. (in Portuguese).
- Baghali, S., Guo, Z., Wei, W., Shahidehpour, M., 2022. Electric vehicles for distribution system load pickup under stressed conditions: a network equilibrium approach. *IEEE Trans. Power Syst.* <https://doi.org/10.1109/TPWRS.2022.3185605>.
- Bi, X., Chipperfield, A.J., Tang, W.K.S., 2021. Coordinating electric vehicle flow distribution and charger allocation by joint optimization. *IEEE Trans. Ind. Inform.* 17 (12), 8112–8121. <https://doi.org/10.1109/TII.2021.3059288>.
- Brady, J., O'Mahony, M., 2016. Modelling charging profiles of electric vehicles based on real-world electric vehicle charging data. *Sustain. Cities Soc.* 26, 203–216. <https://doi.org/10.1016/j.scs.2016.06.014>.
- Bruce da Silva, T., Baptista, P., Santos Silva, C.A., Santos, A., 2022. Assessment of decarbonization alternatives for passenger transportation in Rio de Janeiro, Brazil. *Transp. Res Part D. Transp. Environ.* 103, 103161. <https://doi.org/10.1016/j.trd.2021.103161>.
- Chang, M., Bae, S., Cha, G., Yoo, J., 2021. Aggregated electric vehicle fast-charging power demand analysis and forecast based on LSTM neural network. *Sustainability* 13, 13783. <https://doi.org/10.3390/su132413783>.
- Chen, L., Yang, F., Xing, Q., Wu, S., Wang, R., Chen, J., 2020. Spatial-temporal distribution prediction of charging load for electric vehicles based on dynamic traffic information. *IEEE 4th Conf. Energy Internet Energy Syst. Integr. (EI2)* 1269–1274. <https://doi.org/10.1109/EI250167.2020.9347194>.
- Chen, L.D., Nie, Y.Q., Zhong, Q., 2015. Electric vehicle charging load forecasting model based on trip chain. *J. Electr. Eng.* 30, 216–225.
- Cui, Q., Weng, Y., Tan, C., 2019. Electric vehicle charging station placement method for urban areas. *IEEE Trans. Smart Grid* 10 (6), 6552–6565. <https://doi.org/10.1109/TSG.2019.2907262>.
- Cui, Y., Hu, Z., Duan, X., 2021. Optimal pricing of public electric vehicle charging stations considering operations of coupled transportation and power systems. *IEEE Trans. Smart Grid* 12 (4), 3278–3288. <https://doi.org/10.1109/TSG.2021.3053026>.
- De souza, L.L.P., Lora, E.E., Silva, Palacio, J.C.E., Rocha, M.H., Renó, M.L.G., Venturini, O.J., 2018. Comparative environmental life cycle assessment of conventional vehicles with different fuel options, plug-in hybrid and electric vehicles for a sustainable transportation system in Brazil. *J. Clean. Prod.* 203, 444–468. <https://doi.org/10.1016/j.jclepro.2018.08.236>.
- Ding, Y., Li, X., Jian, S., 2022. Modeling the impact of vehicle-to-grid discharge technology on transport and power systems. *Transp. Res Part D. Transp. Environ.* 105, 103220. <https://doi.org/10.1016/j.trd.2022.103220>.
- Emam, M., 2011. A N. Empir. Formula Calc. Veh. ' Front. Area SAE Tech. Pap. 1, 0763. <https://doi.org/10.4271/2011-01-0763>.
- Esmailirad, S., Ghiasian, A., Rabiee, A., 2021. An Extended M/M/K Queueing Model to Analyze the Profit of a Multiservice Electric Vehicle Charging Station. *IEEE Trans. Veh. Technol.* 70 (4), 3007–3016. <https://doi.org/10.1109/TVT.2021.3063887>.
- EVspecifications, 2022. (<https://www.evspecifications.com/>).
- Faria, R., Moura, P., Delgado, J., de Almeida, T., A., 2012. A sustainability assessment of electric vehicles as a personal mobility system. *Energy Convers. Manag.* 61, 19–30. <https://doi.org/10.1016/j.enconman.2012.02.023>.
- Fazeli, S.S., Venkatachalam, S., Chinnam, R.B., Murat, A., 2021. Two-stage stochastic choice modeling approach for electric vehicle charging station network design in urban communities. *IEEE Trans. Intell. Transp. Syst.* 22 (5), 3038–3053. <https://doi.org/10.1109/TITS.2020.2979363>.
- Fridgen, G., Thimmel, M., Weibelzahl, M., Wolf, L., 2021. Smarter charging: power allocation accounting for travel time of electric vehicle drivers. *Transp. Res. Part D. Transp. Environ.* 97, 102916. <https://doi.org/10.1016/j.trd.2021.102916>.
- Fu, Z., Dong, P., Li, S., Ju, Y., Liu, H., 2021. How blockchain renovate the electric vehicle charging services in the urban area? A case study of Shanghai, China. *J. Clean. Prod.* 315, 128172. <https://doi.org/10.1016/j.jclepro.2021.128172>.
- Ge, X., Shi, L., Fu, Y., Muyeen, S.M., Zhang, Z., He, H., 2020. Data-driven spatial-temporal prediction of electric vehicle load profile considering charging behavior. *Electr. Power Syst. Res.* 187, 106469. <https://doi.org/10.1016/j.epsr.2020.106469>.
- Gruosso, G., Gaiani, G.S., 2019. A model of electric vehicle recharge stations based on cyclic markov chains. *IECON 2019 - 45th Annu. Conf. IEEE Ind. Electron. Soc.* 2586–2591. <https://doi.org/10.1109/IECON.2019.8927724>.
- Haiyang, L., Kun, F., Yu, W., Qie, S., Hailong, L., Yukun, H., Bo, S., Ronald, W., 2019. Characteristics of electric vehicle charging demand at multiple types of location - Application of an agent-based trip chain model. *Energy* 188, 116122. <https://doi.org/10.1016/j.energy.2019.116122>.
- Han, X., Wei, Z., Hong, Z., Zhao, S., 2020. Ordered charge control considering the uncertainty of charging load of electric vehicles based on Markov chain. *Renew. Energy* 161, 419–434. <https://doi.org/10.1016/j.renene.2020.07.013>.
- He, F., Yan, X., Yang, L., Ma, L., 2016. A Traffic congestion assessment method for urban road networks based on speed performance Index. *Procedia Eng.* 137, 425–433. <https://doi.org/10.1016/j.proeng.2016.01.277>.
- Huang, Y., Kockelman, K.M., 2020. Electric vehicle charging station locations: elastic demand, station congestion, and network equilibrium. *Transp. Res Part D. Transp. Environ.* 78, 102179. <https://doi.org/10.1016/j.trd.2019.11.008>.
- IBGE, 2022. Instituto Brasileiro de Geografia e Estatística. (<https://cidades.ibge.gov.br;brasil/sp/campinas>). (in Portuguese).
- Infraestrutura, 2022. Frota de Veículos. (<https://www.gov.br/infraestrutura/pt-br/assuntos/transito/conteudo-denatran/frota-de-veiculos>). (in Portuguese).
- Iversen, E.B., Möller, J.K., Morales, J.M., Madsen, H., 2017. Inhomogeneous markov models for describing driving patterns. *IEEE Trans. Smart Grid* 8 (2), 581–588. <https://doi.org/10.1109/TSG.2016.2520661>.
- Iwafune, Y., Ogimoto, K., Kobayashi, Y., Murai, K., 2020. Driving simulator for electric vehicles using the markov chain monte carlo method and evaluation of the demand response effect in residential houses. *IEEE Access* 8, 47654–47663. <https://doi.org/10.1109/ACCESS.2020.2978867>.
- Kasani, V.S., Tiwari, D., Khalghani, M.R., Solanki, K.S., Solanki, J., 2021. Optimal Coordinated Charging and Routing Scheme of Electric Vehicles in Distribution Grids: real grid cases. *Sustain. Cities Soc.* 73, 103081. <https://doi.org/10.1016/j.scs.2021.103081>.
- Kavianipour, M., Fakhrooosavi, F., Singh, H., Ghamami, M., Zockaie, A., Ouyang, Y., Jackson, R., 2021. Electric vehicle fast charging infrastructure planning in urban networks considering daily travel and charging behavior. *Transp. Res. Part D: Transp. Environ.* 93, 102769. <https://doi.org/10.1016/j.trd.2021.102769>.
- Kumar, N., Kumar, T., Nema, S., Thakur, T., 2022. A comprehensive planning framework for electric vehicles fast charging station assisted by solar and battery based on Queueing theory and non-dominated sorting genetic algorithm-II in a co-ordinated transportation and power network. *J. Energy Storage* 49, 104180. <https://doi.org/10.1016/j.est.2022.104180>.
- Lebrouhi, B.E., Khattari, Y., Lamrani, B., Maaroufi, M., Zeraouli, Y., Kouksou, T., 2021. Key challenges for a large-scale development of battery electric vehicles: a comprehensive review. *J. Energy Storage* 44 (Part B), 103273. <https://doi.org/10.1016/j.est.2021.103273>.
- Li, H., Du, Z., Chen, L., Zhou, B., 2018. A spatial-temporal charging load forecasting modelling of electric vehicles considering urban traffic network. *2018 IEEE Innov. Smart Grid Technol. - Asia (ISGT Asia)* 127–132. <https://doi.org/10.1109/ISGT-Asia.2018.8464795>.
- Li, S., Gu, C., Zeng, X., Zhao, P., Pei, S., 2021. Vehicle-to-grid management for multi-time scale grid power balancing. *Energy* 234, 121201. <https://doi.org/10.1016/j.energy.2021.121201>.
- Liao, J.T., Huang, H.W., Yang, H.T., Li, D., 2021. Decentralized V2G/G2V Scheduling of EV Charging Stations by Considering the Conversion Efficiency of Bidirectional Chargers. *Energies* 14 (4), 962. <https://doi.org/10.3390/en14040962>.
- Lin, Y., Zhang, K., Shen, Z.M., Ye, B., Miao, L., 2019. Multistage large-scale charging station planning for electric buses considering transportation network and power grid. *Transp. Res. Part C: Emerg. Technol.* 107, 423–443. <https://doi.org/10.1016/j.trc.2019.08.009>.
- Mangipinto, A., Lombardi, F., Sanvito, D.S., Pavicević, M., Quoilin, S., Colombo, E., 2022. Impact of mass-scale deployment of electric vehicles and benefits of smart charging across all European countries. *Appl. Energy* 312, 118676. <https://doi.org/10.1016/j.apenergy.2022.118676>.
- Mirzaei, M.J., Kazemi, A., Homaei, O., 2016. A probabilistic approach to determine optimal capacity and location of electric vehicles parking lots in distribution networks. *IEEE Trans. Ind. 12*, 1963–1972. <https://doi.org/10.1109/TII.2015.2482919>.
- Moradzadeh, M., Abdelaziz, M.M.A., 2021. A stochastic optimal planning model for fully green stand-alone PEV charging stations. *IEEE Trans. Transp. Electrification* 7 (4), 2356–2375. <https://doi.org/10.1109/TTE.2021.3069438>.
- Mu, Y., Wu, J., Jenkins, N., Jia, H., Wang, C., 2014. A spatial-temporal model for grid impact analysis of plug-in electric vehicles. *Appl. Energy* 114, 456–465. <https://doi.org/10.1016/j.apenergy.2013.10.006>.
- Muttaqi, K.M., Islam, M.R., Sutanto, D., 2019. Future power distribution grids: integration of renewable energy, energy storage, electric vehicles, superconductor, and magnetic bus. *IEEE Trans. Appl. Supercond.* 29 (2), 1–5. <https://doi.org/10.1109/TASC.2019.2895528>.
- Nguyen, H.N.T., Zhang, C., Mahmud, M.A., 2015. Optimal coordination of G2V and V2G to support power grids with high penetration of renewable energy. *IEEE Trans. Electrification* 1 (2), 188–195. <https://doi.org/10.1109/TTE.2015.2430288>.
- NHTS, 2017. U.S. Department of transportation, National Household Travel Survey. (<https://nhts.ornl.gov/>).
- Open Street Map (OSM). (2024) (<https://www.openstreetmap.org/>).
- Paterakis, N.G., Gibescu, M., 2016. A methodology to generate power profiles of electric vehicle parking lots under different operational strategies. *Appl. Energy* 173, 111–123. <https://doi.org/10.1016/j.apenergy.2016.04.024>.
- Rodríguez-Pajarón, P., Hernández, A., V. Milanović, J., 2021. Probabilistic assessment of the impact of electric vehicles and nonlinear loads on power quality in residential networks. *Int. J. Electr. Power Energy Syst.* 129, 106807. <https://doi.org/10.1016/j.ijepes.2021.106807>.
- Safdarian, F., Lamonte, L., Kargarian, A., Farasat, M., 2019. Distributed optimization-based hourly coordination for V2G and G2V. *IEEE Tex. Power Energy Conf. (TPEC)* 1–6 <https://doi.org/10.1109/TPEC.2019.8662148>.

- Salama, H.S., Said, S.M., Aly, M., Vokony, I., Hartmann, B., 2021. Studying impacts of electric vehicle functionalities in wind energy-powered utility grids with energy storage device. *IEEE Access* 9, 45754–45769. <https://doi.org/10.1109/ACCESS.2021.3066877>.
- Sastry, S., 2013. Evaluating the actual overall efficiency of the car. *Innov. Res. Sci. Eng. Technol., IJIRSET* 2, 1826–1829.
- SEPLAMA, 2022. In Portuguese. Prefeitura Munic. De. Camp. (<https://novo.campinas.sp.gov.br/>).
- Sevdari, K., Calearo, L., Andersen, P.B., Marinelli, M., 2022. Ancillary services and electric vehicles: an overview from charging clusters and chargers technology perspectives. *Renew. Sustain. Energy Rev.* 167, 112666 <https://doi.org/10.1016/j.rser.2022.112666>.
- Shafaqat, J., Liu, J., 2023. Electrical vehicle charging load mobility analysis based on a spatial-temporal method in urban electrified-transportation networks. *Energies* 16, 5178. <https://doi.org/10.3390/en16135178>.
- Shepero, M., Munkhammar, J., 2018. Spatial Markov chain model for electric vehicle charging in cities using geographical information system (GIS) data. *Appl. Energy* 231, 1089–1099. <https://doi.org/10.1016/j.apenergy.2018.09.175>.
- Spencer, S.I., Fu, Z., Apostolaki-Iosifidou, E., Lipman, T.E., 2021. Evaluating smart charging strategies using real-world data from optimized plug-in electric vehicles. *Transp. Res. Part D: Transp. Environ.* 100, 103023 <https://doi.org/10.1016/j.trd.2021.103023>.
- STM, 2022. Secr. De. Estado Dos. Transp. Metrop. (<http://www.stm.sp.gov.br/>) (in Portuguese).
- Straub, F., Maier, O., Göblich, D., Zou, Z., 2023. Forecasting the spatial and temporal charging demand of fully electrified urban private car transportation based on large-scale traffic simulation, 2023. *Green. Energy Intell. Transp.* Volume 2 (Issue 1), 100039. <https://doi.org/10.1016/j.geits.2022.100039>.
- Su, J., Lie, T.T., Zamora, R., 2019. Modeling of large-scale electric vehicles charging demand: a New Zealand case study. *Electr. Power Syst. Res.* 167, 171–182. <https://doi.org/10.1016/j.epsr.2018.10.030>.
- Tang, D., Wang, P., 2016. Probabilistic modeling of nodal charging demand based on spatial-temporal dynamics of moving electric vehicles. *IEEE Trans. Smart Grid* 7 (2), 627–636. <https://doi.org/10.1109/TSG.2015.2437415>.
- Ternel, C., Bouter, A., Melgar, J., 2021. Life cycle assessment of mid-range passenger cars powered by liquid and gaseous biofuels: comparison with greenhouse gas emissions of electric vehicles and forecast to 2030. *Transp. Res. Part D: Transp. Environ.* 97, 102897 <https://doi.org/10.1016/j.trd.2021.102897>.
- Torres, S., Durán, I., Marulanda, A., Pavas, A., Quirós-Tortós, J., 2022. Electric vehicles and power quality in low voltage networks: real data analysis and modeling. *Appl. Energy* 305, 117718. <https://doi.org/10.1016/j.apenergy.2021.117718>.
- USGS, N.A.S.A., 2022. Shuttle Radar Topogr. Mission. 1 arc Second Void-Fill. (<http://earthexplorer.usgs.gov>).
- Wang, D., Gao, J.Y., Li, P., Wang, B., Zhang, C., Saxena, S., 2017. Modeling of plug-in electric vehicle travel patterns and charging load based on trip chain generation. *J. Power Sources* 359, 468–479. <https://doi.org/10.1016/j.jpowsour.2017.05.036>.
- Wang, S., Chen, A., Wang, P., Zhuge, C., 2023. Predicting electric vehicle charging demand using a heterogeneous spatio-temporal graph convolutional network. *Transp. Res. Part C: Emerg. Technol.* Volume 153, 104205 <https://doi.org/10.1016/j.trc.2023.104205>.
- Wang, Y., Infield, D., 2018. Markov chain Monte Carlo simulation of electric vehicle use for network integration studies. *Int. J. Electr. Power Energy Syst.* 99, 85–94. <https://doi.org/10.1016/j.ijepes.2018.01.008>.
- Wimbadi, R.W., Djalante, R., Mori, A., 2021. Urban experiments with public transport for low carbon mobility transitions in cities: a systematic literature review (1990–2020). *Sustain. Cities Soc.* 72, 103023 <https://doi.org/10.1016/j.scs.2021.103023>.
- Xia, Y., Hu, B., Xie, K., Tang, J., Tai, H.M., 2019. An EV charging demand model for the distribution system using traffic property. *IEEE Access* 7, 28089–28099. <https://doi.org/10.1109/ACCESS.2019.2901857>.
- Xiao, D., An, S., Cai, H., Wang, J., Cai, H., 2020. An optimization model for electric vehicle charging infrastructure planning considering queuing behavior with finite queue length. *J. Energy Storage* 29, 101317. <https://doi.org/10.1016/j.est.2020.101317>.
- Xing, Q., Chen, Z., Zhang, Z., Xu, X., Zhang, T., Huang, X., Wang, H., 2020. Urban electric vehicle fast-charging demand forecasting model based on data-driven approach and human decision-making behavior. *Energies* 13, 1412. <https://doi.org/10.3390/en13061412>.
- Xing, Q., Chen, Z., Zhang, Z., Huang, X., Leng, Z., Sun, K., Chen, Y., Wang, H., 2019. Charging demand forecasting model for electric vehicles based on online ride-hailing trip data. *IEEE Access* 7, 137390–137409. <https://doi.org/10.1109/ACCESS.2019.2940597>.
- Yan, J., Zhang, J., Liu, Y., Lv, G., Han, S., Alfonzo, I.E.G., 2020. EV charging load simulation and forecasting considering traffic jams and weather to support the integration of renewables and EVs. *Renew. Energy* 159, 623–641. <https://doi.org/10.1016/j.renene.2020.03.175>.
- Yang, Y., Shun, T., Xiao, X., Jian, Z., Kunyu, L., Jianfeng, W., 2016. Study on charging demand for EV based on stochastic analysis of trip chain. *IET Gener. Transm. Distrib.* 10 (11), 2689–2698. (<https://doi.org/10.1049/iet-gtd.2015.0995>).
- Yi, T., Zhang, C., Lin, T., Liu, J., 2019. Research on the spatial-temporal distribution of electric vehicle charging load demand: a case study in China. *J. Clean. Prod.* Volume 242, 118457 <https://doi.org/10.1016/j.jclepro.2019.118457>.
- Yi, Zhiyan, Liu, Xiaoyue Cathy, Wei, Ran, 2022. Electric vehicle demand estimation and charging station allocation using urban informatics. *Transp. Res. Part D: Transp. Environ.* 106, 103264 <https://doi.org/10.1016/j.trd.2022.103264>.
- Yue, X., Zhuozhen, J., Chenghong, G., Fei, T., Xiangyu, W., Yang, W., 2019. Electric Vehicle Charging in Smart Grid: a Spatial-temporal Simulation Method. *Energy* 189, 116221. <https://doi.org/10.1016/j.energy.2019.116221>.
- Zahedmanesh, A., Muttaqi, K.M., Sutanto, D., 2021. A cooperative energy management in a virtual energy hub of an electric transportation system powered by PV generation and energy storage. *IEEE Trans. Transp. Electrification* 7 (3), 1123–1133. <https://doi.org/10.1109/TTE.2021.3055218>.
- Zhang, J., Yan, J., Liu, Y., Zhang, H., Lv, G., 2020. Daily electric vehicle charging load profiles considering demographics of vehicle users. *Appl. Energy* 274, 115063. <https://doi.org/10.1016/j.apenergy.2020.115063>.
- Zhang, J., Wang, Z., Miller, E.J., Cui, D., Liu, P., Zhang, Z., 2023. Charging demand prediction in Beijing based on real-world electric vehicle data. *J. Energy Storage* Volume 57, 106294. <https://doi.org/10.1016/j.est.2022.106294>.
- Zhang, Q., Wang, Z., Tan, W., Liu, H., Li, C., 2018. Spatial-temporal distribution prediction of charging load for electric vehicle based on MDP random path simulation. *Power Syst.* 42 (20), 59–73. <https://doi.org/10.7500/AEPS20171117007>.
- Zhang, X., Chan, K.W., Li, H., Wang, H., Qiu, J., Wang, G., 2021. Deep-learning-based probabilistic forecasting of electric vehicle charging load with a novel queuing model. *IEEE Trans. Cybern.* 51 (6), 3157–3170. <https://doi.org/10.1109/TCYB.2020.2975134>.
- Zhao, Y., Wang, Z., Max, Z.J., Sun, F., 2021. Data-driven framework for large-scale prediction of charging energy in electric vehicles. *Appl. Energy* 282, 116175. <https://doi.org/10.1016/j.apenergy.2020.116175>.
- Zhu, L., Ge, Y., Wang, K., Fan, Y., Ma, X., Zhang, L., 2023. Spatial-Temporal Electric Vehicle Charging Demand Forecasting: A GTrans Approach. https://doi.org/10.1007/978-981-99-5847-4_25.
- Zou, Y., Zhao, J., Gao, X., Chen, Y., Tohidi, A., 2020. Experimental results of electric vehicles effects on low voltage grids. *J. Clean. Prod.* 255, 120270 <https://doi.org/10.1016/j.jclepro.2020.120270>.